Journal of Computational Methods in Molecular Design, 2014, 4 (4):79-120

Scholars Research Library
(http://scholarsresearchlibrary.com/archive.html)

ISSN : 2231- 3176
CODEN (USA): JCMMDA

A Theoretical Study of the Relationships between Electronic Structure and Cytotoxicity of a group of N^2-alkylated Quaternary β-Carbolines against nine Tumoral Cell Lines

Fernando Gatica-Díaz and Juan S. Gómez-Jeria*

Quantum Pharmacology Unit, Department of Chemistry, Faculty of Sciences, University of Chile. Las Palmeras 3425, Santiago 7800003, Chile

---

ABSTRACT

Here we present the results of a study relating molecular/electronic structure with cytotoxicity for a group of N^2-alkylated quaternary β-carbolines against nine tumoral cell lines. The electronic structure of all systems was calculated at the B3LYP/6-31G(d,p) level. Statistically significant results were obtained for almost all tumoral cell lines. The analysis of the proposed pharmacophores allows detecting several atoms that can be used as targets for substitution and control of cytotoxicity.

Keywords: Tumoral cells, cancer, cytotoxicity, QSAR, β-carbolines, MCF-7, HepG2, 22RV1, HT-29, 769-P, A375, SK-OV-3, Eca-109, BGC-823.

INTRODUCTION

β-carboline (9*H*-pyrido[3,4-*b*]indole, norharmane) is a nitrogen containing heterocycle. It is also the prototype of a set of compounds called β-carbolines. β-carboline alkaloids are naturally occurring in plants and animals, and display a wide range of pharmacological and biological activities including antimicrobial, antioxidant, antitumoral and antiviral actions [1, 2]. They also exert a diversity of neurological, physiological and psychoactive effects such as antidepressant actions, changes in body temperature, convulsion, effects on drug withdrawal and appetite, modification of brain neurotransmitters and vascular relaxation . Norharman and harman have been implicated in a number of human diseases including addiction, cancer, Parkinson's disease and tremor. β-carboline is a benzodiazepine receptor inverse agonist and can consequently have anxiogenic, convulsive and memory enhancing effects. As components of the liana *Banisteriopsis caapi*, harmine, harmaline and tetrahydroharmine play a critical role in the effects of the indigenous psychedelic preparation Ayahuasca [3-7] upon oral ingestion by reversibly inhibiting the monoamine oxidase enzyme. Several groups of β-carboline derivatives have been synthesized and tested for diverse biological activities [8-40]. During the last years an intensive research has been carried out on the antitumor/cytotoxic properties of these molecular systems [8, 14, 19, 22, 41-54]. In this paper we present the results of an analysis between the electronic and conformational properties of a group of N^2-alkylated quaternary β-carbolines and their cytotoxic activity against nine tumoral cell lines.

MATERIALS AND METHODS

MODEL AND CALCULATIONS

Taking into consideration that the model-based method used here has been described and discussed in great detail in several papers, we present only a short standard summary [55-61]. The cytotoxicity, expressed as IC_{50}, is a linear function of several local atomic reactivity indices (LARIs) and has the form:

$$\log(IC_{50}) = a + bM_{D_i} + c\log\left[\sigma_{D_i} / (ABC)^{1/2}\right] + \sum_j \left[e_j Q_j + f_j S_j^E + s_j S_j^N\right] +$$
$$+ \sum_j \sum_m \left[h_j(m) F_j(m) + x_j(m) S_j^E(m)\right] + \sum_j \sum_{m'} \left[r_j(m') F_j(m') + t_j(m') S_j^N(m')\right] +$$
$$+ \sum_j \left[g_j \mu_j + k_j \eta_j + o_j \omega_j + z_j \varsigma_j + w_j Q_j^{\max}\right] + \sum_{B=1}^{W} O_B \qquad (1)$$

where ABC the product of the drug's moment of inertia about the three principal axes of rotation, M is the drug's mass and σ its symmetry number. O_B is the orientational parameter of the B-th substituent. The other terms are local atomic reactivity indices (LARIs) and are related to the kinds of interactions between the drug atoms and the site. We refer the reader to the several papers discussing their physical meaning [60-64]. Below we shall discuss the specific LARIs appearing in the resulting equations. The use of this method has given excellent results in the study of the equilibrium constant for several kinds of drug-receptor interactions [58, 65-80]. Recently the method was extended to the study of very different biological activities with a remarkable success [62, 64, 81-99]. The selected β-carbolines and their experimental cytotoxic activities ([54]) are shown in Fig. 1 and Tables 1-3.

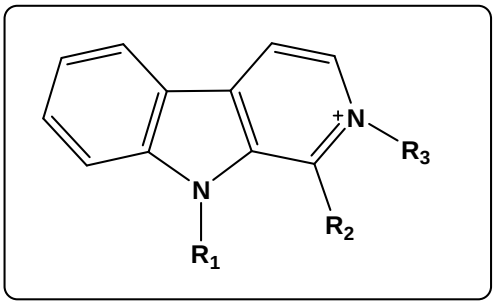

Figure 1. Structure of β-carbolines.

Table 1. β-carbolines.

Mol.	R_1	R_2	R_3
1	$-CH_3$	-H	$-CH_2C_6H_5$
2	$-C_2H_5$	-H	$-CH_2C_6H_5$
3	$-CH(CH_3)_2$	-H	$-CH_2C_6H_5$
4	$-CH_2CH{=}CH_2$	-H	$-CH_2C_6H_5$
5	n-C_4H_9	-H	$-CH_2C_6H_5$
6	$-CH_2CH(CH_3)_2$	-H	$-CH_2C_6H_5$
7	n-C_6H_{13}	-H	$-CH_2C_6H_5$
8	n-C_8H_{17}	-H	$-CH_2C_6H_5$
9	$-CH_2C_6H_5$	-H	$-CH_2C_6H_5$
10	-*p*-$CH_2C_6H_4F$	-H	$-CH_2C_6H_5$
11	-*m*-$CH_2C_6H_4Cl$	-H	$-CH_2C_6H_5$
12	-*p*-$CH_2C_6H_4OCH_3$	-H	$-CH_2C_6H_5$
13	$-(CH_2)_3C_6H_5$	-H	$-CH_2C_6H_5$
14	$-(CH_2)_3C_6H_5$	-H	$-CH_3$
15	$-(CH_2)_3C_6H_5$	-H	$-C_2H_5$
16	$-(CH_2)_3C_6H_5$	-H	n-C_4H_9
17	$-(CH_2)_3C_6H_5$	-H	n-C_6H_{13}
18	$-(CH_2)_3C_6H_5$	-H	n-C_8H_{17}

19	$-(CH_2)_3C_6H_5$	-H	$n\text{-}C_{10}H_{21}$
20	$-(CH_2)_3C_6H_5$	-H	$-p\text{-}CH_2C_6H_4F$
21	$-(CH_2)_3C_6H_5$	-H	$-m\text{-}CH_2C_6H_4Cl$
22	$-(CH_2)_3C_6H_5$	-H	$-p\text{-}CH_2C_6H_4NO_2$
23	$-(CH_2)_3C_6H_5$	-H	$-(CH_2)_2C_6H_5$
24	$-(CH_2)_3C_6H_5$	-H	$-(CH_2)_3C_6H_5$
25	$-(CH_2)_3C_6H_5$	$-CH_3$	$-CH_2C_6H_5$
26	$-(CH_2)_3C_6H_5$	$-C_2H_5$	$-CH_2C_6H_5$
27	$-(CH_2)_3C_6H_5$	$-p\text{-}C_6H_5OCH_3$	$-CH_2C_6H_5$
28	$-(CH_2)_3C_6H_5$	$-C_4H_3S$	$-CH_2C_6H_5$

Table 2. Cytotoxic activities of β-carbolines*.

Mol.	$\log(IC_{50})$	$\log(IC_{50})$	$\log(IC_{50})$	$\log(IC_{50})$	$\log(IC_{50})$
	MCF-7	HepG2	22RV1	HT-29	769-P
1	---	---	0.92	1.77	1.35
2	---	---	0.75	---	1.59
3	1.74	1.77	0.56	---	1.49
4	1.86	1.83	----	---	1.34
5	1.53	1.46	---	1.92	1.30
6	1.59	1.56	0.98	1.94	1.06
7	1.05	1.14	---	1.20	0.43
8	0.61	0.81	0.46	1.04	---
9	1.27	1.54	0.76	1.63	0.94
10	1.25	1.37	0.54	1.46	0.78
11	1.31	1.22	0.62	1.43	0.54
12	1.27	1.20	0.68	1.28	0.88
13	1.16	0.90	0.51	0.88	0.69
14	1.88	1.96	0.63	1.99	1.30
15	1.99	1.96	0.40	1.73	1.53
16	1.59	1.66	0.53	1.80	1.13
17	0.59	0.63	0.34	0.36	0.40
18	0.46	0.67	0.63	1.27	---
19	---	---	0.84	1.50	---
20	0.99	1.02	0.63	0.96	1.16
21	1.16	1.28	0.99	1.22	1.34
22	1.39	1.30	0.75	1.10	0.92
23	1.10	1.15	0.60	0.52	1.15
24	0.57	0.60	0.69	0.53	0.52
25	0.85	0.76	0.26	1.16	0.72
26	0.57	0.68	0.57	1.03	0.48
27	0.34	0.52	0.26	0.38	---
28	1.47	1.56	0.92	1.50	1.16

** MCF-7: breast carcinoma, HepG2: liver carcinoma, 22RV1: prostate carcinoma, HT-29: colon carcinoma, 769-P: renal carcinoma.*

Table 3. Cytotoxic activities of β-carbolines*.

Mol.	$\log(IC_{50})$	$\log(IC_{50})$	$\log(IC_{50})$	$\log(IC_{50})$
	A375	SK-OV-3	Eca-109	BGC-823
1	1.57	1.74	1.98	1.12
2	1.73	1.44	1.56	---
3	1.39	0.82	0.88	1.79
4	1.05	1.10	1.33	---
5	1.29	0.67	0.93	1.83
6	1.45	1.44	1.55	1.78
7	0.83	0.86	1.14	0.72
8	0.49	0.51	0.71	0.40
9	0.89	1.23	1.51	1.59
10	0.67	1.02	1.55	0.80
11	0.85	0.90	1.37	1.31
12	0.98	1.30	1.73	1.25
13	0.94	0.64	1.07	0.93
14	1.62	---	1.78	1.61
15	1.65	---	1.74	1.94
16	1.09	1.20	1.62	1.19
17	0.46	---	0.40	0.36

18	---	0.77	1.36	0.87
19	---	1.76	1.37	1.76
20	1.02	1.09	0.72	0.91
21	1.39	1.14	0.90	0.99
22	1.09	1.24	0.88	1.60
23	1.09	0.92	0.91	1.02
24	0.51	1.03	0.72	0.97
25	0.93	0.88	0.83	0.84
26	0.77	---	0.71	---
27		0.72	1.09	0.51
28	1.45	1.16	1.43	0.60

** A375: malignant melanoma, SK-OV-3: ovarian carcinoma, Eca-109: esophageal carcinoma, BGC-823: gastric carcinoma.*

A preliminary analysis showed that no statistically significant results could be obtained for the whole set. Therefore, we divided the molecules in two subsets denoted IA and IB. Figure 2 and Table 4 show the group IA of molecules and Fig. 3 and Table 5 show the group IB. Note that some β-carbolines belong to both subsets.

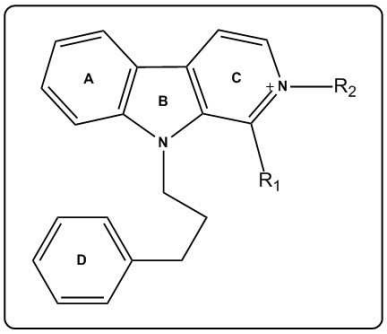

Figure 2. Structure of molecules of group IA of β-carbolines.

Table 4. Molecules of group IA of β-carbolines.

Mol.	R_1	R_2
13	-H	$-CH_2C_6H_5$
14	-H	$-CH_3$
15	-H	$-C_2H_5$
16	-H	$n-C_4H_9$
17	-H	$n-C_6H_{13}$
18	-H	$n-C_8H_{17}$
19	-H	$n-C_{10}H_{21}$
20	-H	$-p-CH_2C_6H_4F$
21	-H	$-m-CH_2C_6H_4Cl$
22	-H	$-p-CH_2C_6H_4NO_2$
23	-H	$-(CH_2)_2C_6H_5$
24	-H	$-(CH_2)_3C_6H_5$
25	$-CH_3$	$-CH_2C_6H_5$
26	$-C_2H_5$	$-CH_2C_6H_5$
27	$-p-C_6H_5OCH_3$	$-CH_2C_6H_5$
28	$-C_4H_3S$	$-CH_2C_6H_5$

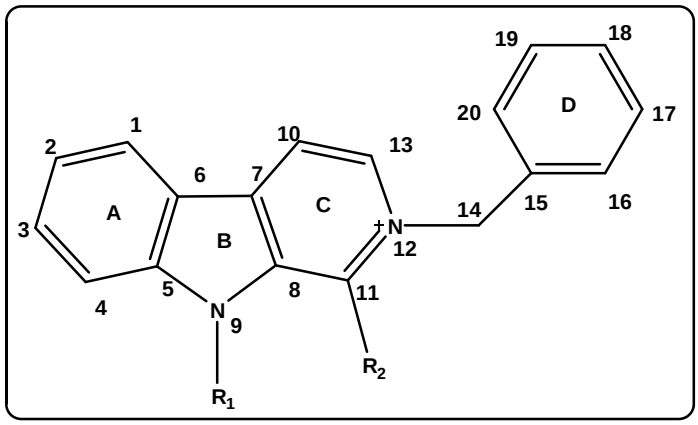

Figure 3. Structure of molecules of group IB of β-carbolines.

Table 5. Molecules of group IB of β-carbolines.

Mol.	R_1	R_2
1	$-CH_3$	-H
2	$-C_2H_5$	-H
3	$-CH(CH_3)_2$	-H
4	$-CH_2CH=CH_2$	-H
5	n-C_4H_9	-H
6	$-CH_2CH(CH_3)_2$	-H
7	n-C_6H_{13}	-H
8	n-C_8H_{17}	-H
9	$-CH_2C_6H_5$	-H
10	-*p*-$CH_2C_6H_4F$	-H
11	-*m*-$CH_2C_6H_4Cl$	-H
12	-*p*-$CH_2C_6H_4OCH_3$	-H
13	$-(CH_2)_3C_6H_5$	-H
20	$-(CH_2)_3C_6H_5$	-H
21	$-(CH_2)_3C_6H_5$	-H
22	$-(CH_2)_3C_6H_5$	-H
25	$-(CH_2)_3C_6H_5$	$-CH_3$
26	$-(CH_2)_3C_6H_5$	$-C_2H_5$
27	$-(CH_2)_3C_6H_5$	-*p*-$C_6H_5OCH_3$
28	$-(CH_2)_3C_6H_5$	$-C_4H_3S$

METHODS, MODELS AND CALCULATIONS

We carried out all the numerical calculations with the same methodology usually employed in this Unit. Briefly, geometries were fully optimized and a single point calculation was performed with the Gaussian program [100]. The local atomic reactivity indices were calculated from the single point log file with the D-Cent-QSAR software with correction of the anomalous electron populations that sometimes are produced by the Mulliken population analysis [101, 102]. The cationic form was used for all calculations. Orientational parameters were calculated as usual [58, 59]. For both, groups IA and IB, a common skeleton was defined. They are depicted in Figs. 4 and 5.

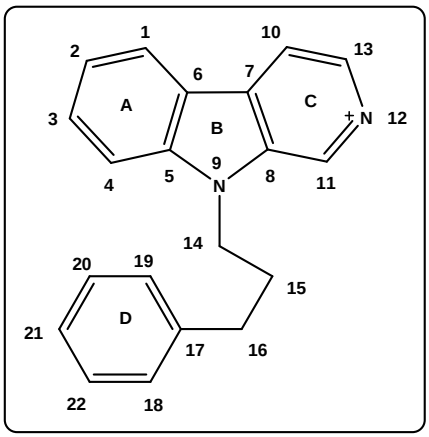

Figure 4. Common skeleton for group IA of β-carbolines.

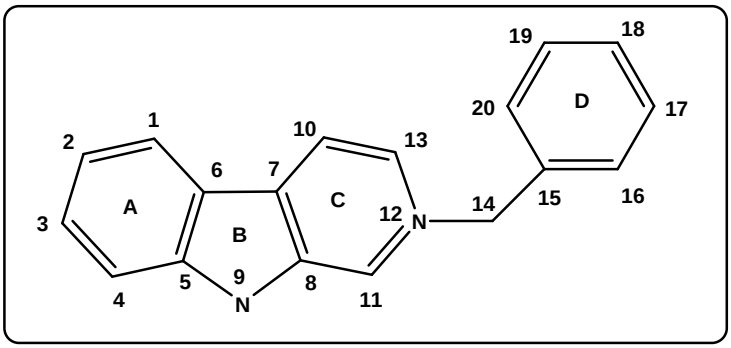

Figure 5. Common skeleton for group IB of β-carbolines.

For each group and cell line a Linear Multiple Regression Analysis (LMRA) was carried out with the Statistica software [103]. The dependent variable is log(IC_{50}) and the dependent ones are the set of LARIs belonging to the corresponding common skeleton. Note that in this kind of model statistics is employed as a servant and not as a queen [104]. It is worth to mention that the method successfully works if and only if every molecule of the set exerts its ultimate biological activity throughout the same mechanism or mechanisms. A detailed explanation of the building of the matrix for LMRA is given in other papers [80, 105].

RESULTS

The final equations relate the *variation* of the cytotoxicity through the family of molecules with the simultaneous *variation* of one or more local atomic reactivity indices. Thus, any index making a constant contribution will not appear in the equation. Given that no significant correlations were detected between the independent variables, the Tables showing the squared correlation coefficients for the variables appearing in the various equations are not shown (they are available on request).

Results for the MCF-7 Cell Line

Group IA results

The equation obtained was:

$$\log(IC_{50}) = 0.66 + 21.86F_6(LUMO)^* - 0.002S_{10}^N + 1.25F_{18}(HOMO-2)^* - \\ -2.74F_8(HOMO-2)^* \quad (2)$$

with n=15, R=0.96, R^2=0.93, adj-R^2=0.90, F(4,10)=31.43 (p<0.000001), SD=0.10. No outliers were detected and no residuals fall outside the ±2σ limits. Here, F_6(LUMO)* is the Fukui index of the lowest vacant MO localized on atom 6, S_N^{10} is the total atomic nucleophilic superdelocalizability of atom 10, F_{18}(HOMO-2)* is the Fukui index of

the third highest occupied MO localized on atom 18 and F_8(HOMO-2)* is the Fukui index of the third occupied MO localized on atom 8. Table 6 shows the beta coefficients and the results of the t-test for significance of coefficients. Fig. 6 displays the plot of observed *vs.* calculated log(IC_{50}) values. The associated statistical parameters of Eq. 2 indicate that this equation is statistically significant and that the variation of the numerical value of a group of four local atomic reactivity indices of atoms of the common skeleton explains about 90% of the variation of the cytotoxicity.

Table 6. Beta coefficients and *t*-test for significance of coefficients in Eq. 2.

	Beta	t(10)	p-level
$F_6(LUMO)*$	0.83	8.97	<0.000004
S_{10}^N	-0.62	-6.36	<0.00008
$F_{18}(HOMO-2)*$	0.39	4.09	<0.002
$F_8(HOMO-2)*$	-0.29	-2.91	<0.02

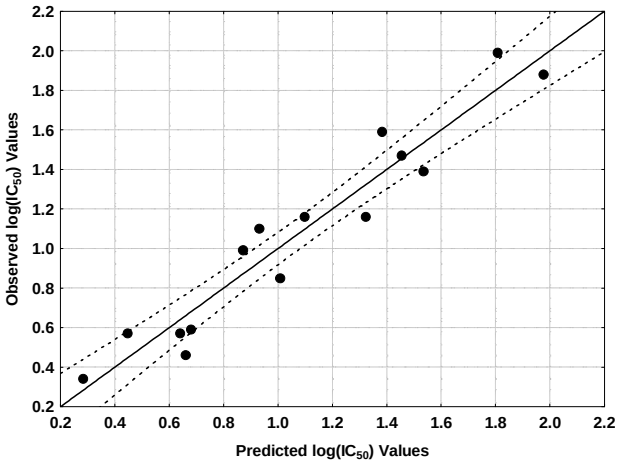

Fig. 6. Observed *vs.* calculated values (Eq. 2) of log (IC_{50}). Dashed lines denote the 95% confidence interval.

Group IB results

With the whole set (n=18) it was not possible to obtain a statistically significant equation. Employing a methodology that gave good results in other studies, we discarded the molecule having the smallest cytotoxicity. With this reduced set we obtained the following equation:

$$\log(IC_{50}) = 5.15 + 28.75S_4^N(LUMO)* - 2.76F_{14}(LUMO)* - 0.0002\phi_{R1} + \\ +1.02Q_9^{\max} - 0.14S_{18}^N(LUMO+1)* \quad (3)$$

with n=17, R=0.97, R^2=0.95, adj-R^2=0.93, F(5,11)=41.90 (p<0.000001) and SD=0.10. No outliers were detected and no residuals fall outside the ±2σ limits. Here, $S_4^N(LUMO)*$ is the nucleophilic superdelocalizability of the lowest vacant MO localized on atom 4, $F_{14}(LUMO)*$ is the Fukui index of the lowest vacant MO localized on atom 14, ϕ_{R1} is the orientational parameter of the R_1 substituent, $Q_9^{\max}$ is the maximal amount of electronic charge atom 9 may receive and $S_{18}^N(LUMO+1)*$ is the nucleophilic superdelocalizability of the second lowest vacant MO localized on atom 18. Table 7 shows the beta coefficients and the results of the t-test for significance of coefficients. Fig. 7 displays the plot of observed *vs.* calculated log(IC_{50}) values. The associated statistical parameters of Eq. 3 indicate that this equation is statistically significant and that the variation of the numerical value of a group of five

local atomic reactivity indices of atoms of the common skeleton explains about 93% of the variation of the cytotoxicity.

Table 7. Beta coefficients and *t*-test for significance of coefficients in Eq. 3.

	Beta	t(11)	p-level
$S_4^N(LUMO)*$	0.85	9.12	<0.000002
$F_{14}(LUMO)*$	-0.48	-5.58	<0.0002
ϕ_{R1}	-0.59	-7.44	<0.00001
$Q_9^{\max}$	0.26	3.13	<0.01
$S_{18}^N(LUMO+1)*$	-0.44	-5.63	<0.0002

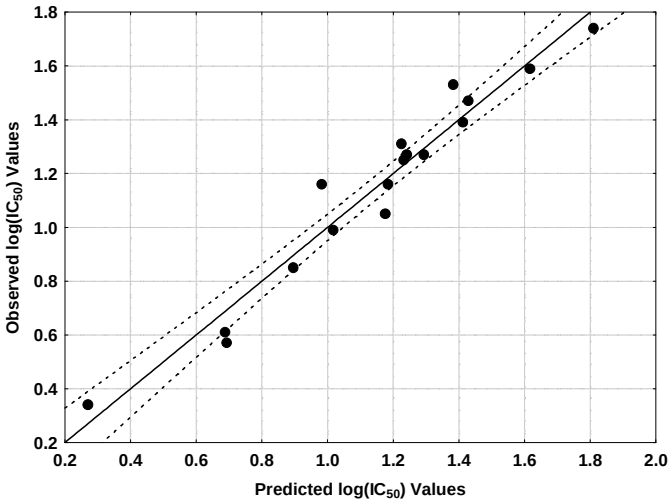

Figure 7. Observed *vs.* calculated values (Eq. 3) of log (IC_{50}). Dashed lines denote the 95% confidence interval.

Results for the HepG2 Cell Line

Group IA results

The best equation obtained is:

$$\log(IC_{50}) = 25.13 + 13.14S_7^N(LUMO)* - 0.0002\phi_{R2} + 3.27F_{16}(HOMO-1)* - \\ -2.87S_8^N(LUMO+2)* + 0.06S_{19}^N(LUMO)* \quad (4)$$

with n=15, R=0.99, R^2=0.98, adj-R^2=0.97, F(5,9)=85.13 (p<0.000001) and SD=0.09. No outliers were detected and no residuals fall outside the ±2σ limits. Here, $S_7^N(LUMO)*$ is the nucleophilic superdelocalizability of the lowest vacant MO localized on atom 7, ϕ_{R2} is the orientational factor of the R_2 substituent, $F_{16}(HOMO-1)*$ is the Fukui index of the second highest occupied MO localized on atom 16, $S_8^N(LUMO+2)*$ is the nucleophilic superdelocalizability of the third lowest vacant MO localized on atom 8 and $S_{19}^N(LUMO)*$ is the nucleophilic superdelocalizability of the lowest vacant MO localized on atom 19. Table 8 shows the beta coefficients and the results of the t-test for significance of coefficients. Fig. 8 displays the plot of observed *vs.* calculated log(IC_{50}) values. The associated statistical parameters of Eq. 4 indicate that this equation is statistically significant and that the variation of the numerical value of a group of five local atomic reactivity indices of atoms of the common skeleton explains about 97% of the variation of the cytotoxicity.

Table 8. Beta coefficients and *t*-test for significance of coefficients in Eq. 4.

	Beta	t(9)	p-level
$S_7^N(LUMO)*$	0.83	15.77	<0.0000001
ϕ_{R2}	-0.55	-10.44	<0.000002
$F_{16}(HOMO-1)*$	0.63	10.72	<0.000002
$S_8^N(LUMO+2)*$	-0.33	-5.65	<0.0003
$S_{19}^N(LUMO)*$	0.20	3.90	<0.004

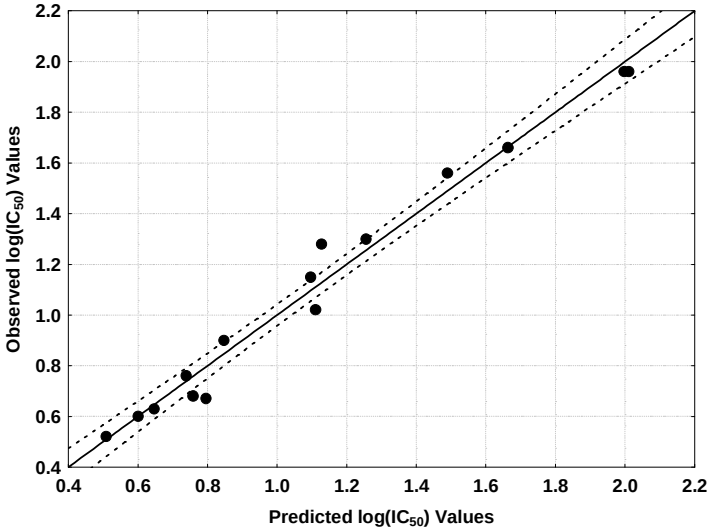

Fig. 8. Observed *vs.* calculated values (Eq. 4) of log (IC_{50}). Dashed lines denote the 95% confidence interval.

Table 9. Beta coefficients and *t*-test for significance of coefficients in Eq. 5.

	Beta	t(13)	p-level
ϕ_{R1}	-0.82	-10.09	<0.0000001
$S_9^N(LUMO)*$	0.70	8.11	<0.000002
η_{18}	-0.51	-5.21	<0.0002
$F_4(HOMO-2)*$	0.23	3.27	<0.006

Group IB results

The best equation obtained is:

$$\log(IC_{50}) = 10.49 - 0.0002\phi_{R1} + 33.62S_9^N(LUMO)* - 0.53\eta_{18} + 1.68F_4(HOMO-2)* \quad (5)$$

with n=15, R=0.99, R^2=0.98, adj-R^2=0.97, F(5,9)=85.13 (p<0.000001) and SD=0.09. No outliers were detected and no residuals fall outside the ±2σ limits. Here, ϕ_{R1} is the orientational parameter of the R_1 substituent, $S_9^N(LUMO)*$ is the nucleophilic superdelocalizability of the lowest vacant MO localized on atom 9, η_{18} is the local atomic hardness of atom 18 and $F_4(HOMO-2)*$ is the Fukui index of the third highest occupied MO localized on atom 4. Table 9 shows the beta coefficients and the results of the t-test for significance of coefficients. Fig. 9 displays the plot of observed *vs.* calculated log(IC_{50}) values. The associated statistical parameters of Eq. 5 indicate that this equation is statistically significant and that the variation of the numerical value of a group of four

local atomic reactivity indices of atoms of the common skeleton explains about 97% of the variation of the cytotoxicity.

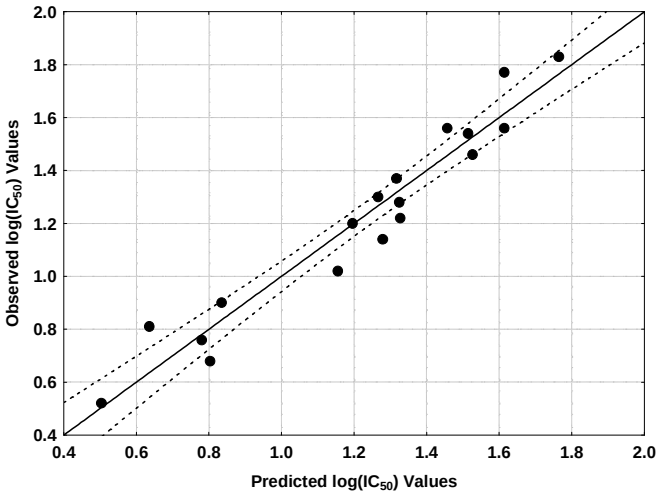

Fig. 9. Observed *vs.* calculated values (Eq. 5) of log (IC_{50}). Dashed lines denote the 95% confidence interval.

Results for the 22RV1 Cell Line

Group IA results

The best equation obtained is:

$$\log(IC_{50}) = -3.85 + 0.77F_{17}(HOMO-2)^* + 20.85S_9^N(LUMO)^* + 51.29s_{18} + \\ +0.33S_{11}^E(HOMO-2)^* \quad (6)$$

with n=18, R=0.97, R^2=0.94, adj-R^2=0.92, F(4,13)=47.88 (p<0.000001) and SD=0.11. No outliers were detected and no residuals fall outside the ±2σ limits. Here, $F_{17}(HOMO-2)^*$ is the Fukui index of the third highest occupied MO localized on atom 17, $S_9^N(LUMO)^*$ is the nucleophilic superdelocalizability of the lowest vacant MO localized on atom 9, s_{18} is the local atomic softness of atom 9 and $S_{11}^E(HOMO-2)^*$ is the electrophilic superdelocalizability of the third highest occupied MO localized on atom 11. Table 10 shows the beta coefficients and the results of the t-test for significance of coefficients. Fig. 10 displays the plot of observed *vs.* calculated log(IC_{50}) values. The associated statistical parameters of Eq. 6 indicate that this equation is statistically significant and that the variation of the numerical value of a group of four local atomic reactivity indices of atoms of the common skeleton explains about 92% of the variation of the cytotoxicity.

Table 10. Beta coefficients and *t*-test for significance of coefficients in Eq. 6.

	Beta	t(10)	p-level
$F_{17}(HOMO-2)^*$	0.35	3.20	<0.009
$S_9^N(LUMO)^*$	0.91	7.64	<0.00002
s_{18}	0.66	5.23	<0.0004
$S_{11}^E(HOMO-2)^*$	0.42	3.54	<0.005

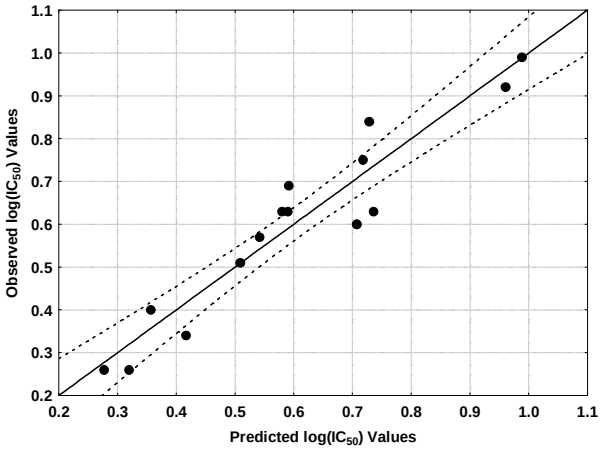

Fig. 10. Observed *vs.* calculated values (Eq. 6) of log (IC_{50}). Dashed lines denote the 95% confidence interval.

Group IB results

The best equation obtained is:

$$\log(IC_{50}) = 7.20 + 22.08 S_9^N(LUMO)^* - 0.42\eta_{19} + 0.07 S_4^N(LUMO+2)^* - \\ -0.00005\phi_{R1} - 0.40 F_{19}(HOMO-2)^* \quad (7)$$

with n=17, R=0.95, R^2=0.90, adj-R^2=0.86, F(5,11)=20.38 (p<0.00003) and SD=0.08. No outliers were detected and no residuals fall outside the ±2σ limits. Here, $S_9^N(LUMO)^*$ is the nucleophilic superdelocalizability of the lowest vacant MO localized on atom 9, η_{19} is the local atomic hardness of atom 19, $S_4^N(LUMO+2)^*$ is the nucleophilic superdelocalizability of the third lowest vacant MO localized on atom 4, ϕ_{R1} is the orientational parameter of the R_1 substituent and $F_{19}(HOMO-2)^*$ is the Fukui index of the third highest occupied MO localized on atom 19. Table 11 shows the beta coefficients and the results of the t-test for significance of coefficients. Fig. 11 displays the plot of observed *vs.* calculated log(IC_{50}) values. The associated statistical parameters of Eq. 7 indicate that this equation is statistically significant and that the variation of the numerical value of a group of four local atomic reactivity indices of atoms of the common skeleton explains about 86% of the variation of the cytotoxicity.

Table 11. Beta coefficients and *t*-test for significance of coefficients in Eq. 7.

	Beta	t(11)	p-level
$S_9^N(LUMO)^*$	0.82	6.14	<0.00007
η_{19}	-0.67	-6.06	<0.00008
$S_4^N(LUMO+2)^*$	0.58	4.30	<0.001
ϕ_{R1}	-0.34	-3.44	<0.006
$F_{19}(HOMO-2)^*$	-0.28	-2.55	<0.03

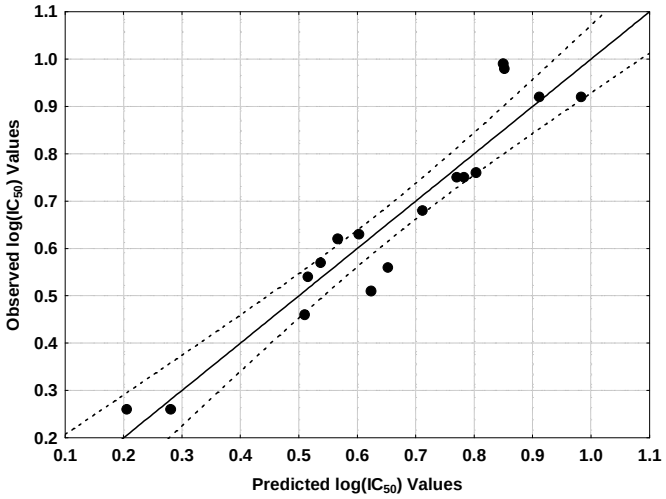

Fig. 11. Observed *vs.* calculated values (Eq. 7) of log (IC_{50}). Dashed lines denote the 95% confidence interval.

Results for the HT-29 Cell Line

Group IA results

With the whole set (n=16) it was not possible to obtain a statistically significant equation. When we discarded the molecule having the smallest cytotoxicity, we obtained the following equation:

$$\log(IC_{50}) = 1.68 - 1.60S_{17}^{E}(HOMO-2)^{*} + 33.49S_{10}^{E}(HOMO)^{*} - 0.08S_{18}^{N}(LUMO+1)^{*} + \\ +0.002S_{14}^{N} \quad (8)$$

with n=15, R=0.96, R^2=0.92, adj-R^2=0.88, F(4,10)=20.38 (p<0.0002) and SD=0.16. No outliers were detected and no residuals fall outside the ±2σ limits. Here, $S_{17}^{E}(HOMO-2)^{*}$ is the electrophilic superdelocalizability of the third highest occupied MO localized on atom 17, $S_{10}^{E}(HOMO)^{*}$ is the electrophilic superdelocalizability of the highest occupied MO localized on atom 10, $S_{18}^{N}(LUMO+1)^{*}$ is the nucleophilic superdelocalizability of the second lowest vacant MO localized on atom 18 and S_{14}^{N} is the nucleophilic superdelocalizability of atom 14. Table 12 shows the beta coefficients and the results of the t-test for significance of coefficients. Fig. 12 displays the plot of observed *vs.* calculated log(IC_{50}) values. The associated statistical parameters of Eq. 8 indicate that this equation is statistically significant and that the variation of the numerical value of a group of four local atomic reactivity indices of atoms of the common skeleton explains about 88% of the variation of the cytotoxicity.

Table 12. Beta coefficients and *t*-test for significance of coefficients in Eq. 8.

	Beta	t(10)	p-level
$S_{17}^{E}(HOMO-2)^{*}$	-0.79	-8.05	<0.00001
$S_{10}^{E}(HOMO)^{*}$	0.67	6.71	<0.00005
$S_{18}^{N}(LUMO+1)^{*}$	-0.41	-3.98	<0.003
S_{14}^{N}	0.29	3.08	<0.01

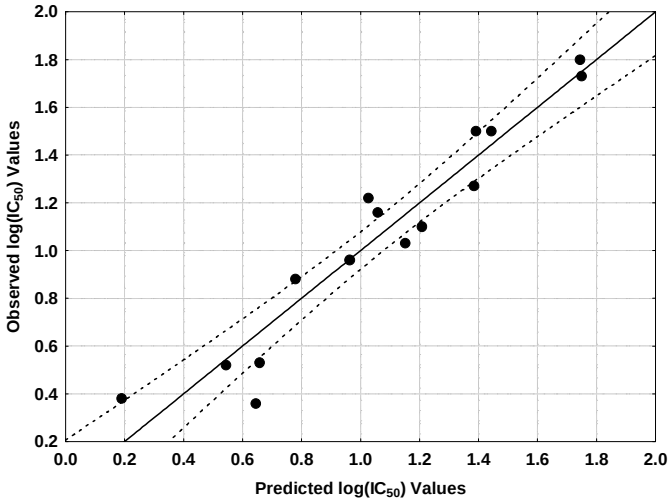

Fig. 12. Observed *vs.* calculated values (Eq. 8) of log (IC_{50}). Dashed lines denote the 95% confidence interval.

Group IB results

For the whole set (n=17) no satisfactory equation was obtained. Using the same procedure used before, and after extracting two molecules from the set, the following equation was obtained:

$$\log(IC_{50}) = 6.98 + 31.80 S_9^N(LUMO)^* - 0.54 F_{19}(LUMO+2)^* - 0.0001\phi_{R1} + \\ + 0.84 F_{15}(LUMO+2)^* \quad (9)$$

with n=15, R=0.96, R^2=0.93, adj-R^2=0.90, F(4,10)=32.67 (p<0.00001) and SD=0.11. No outliers were detected and no residuals fall outside the ±2σ limits. Here, $S_9^N(LUMO)^*$ is the nucleophilic superdelocalizability of the lowest vacant MO localized on atom 9, $F_{19}(LUMO+2)^*$ is the Fukui index of the third lowest vacant MO localized on atom 19, ϕ_{R1} is the orientational parameter of the R_1 substituent and $F_{15}(LUMO+2)^*$ is the Fukui index of the third lowest vacant MO localized on atom 15. Table 13 shows the beta coefficients and the results of the t-test for significance of coefficients. Fig. 13 displays the plot of observed *vs.* calculated log(IC_{50}) values. The associated statistical parameters of Eq. 9 indicate that this equation is statistically significant and that the variation of the numerical value of a group of four local atomic reactivity indices of atoms of the common skeleton explains about 90% of the variation of the cytotoxicity.

Table 13. Beta coefficients and *t*-test for significance of coefficients in Eq. 9.

	Beta	t(10)	p-level
$S_9^N(LUMO)^*$	0.80	7.94	<0.00001
$F_{19}(LUMO+2)^*$	-0.35	-3.66	<0.004
ϕ_{R1}	-0.39	-4.25	<0.002
$F_{15}(LUMO+2)^*$	0.27	2.85	<0.02

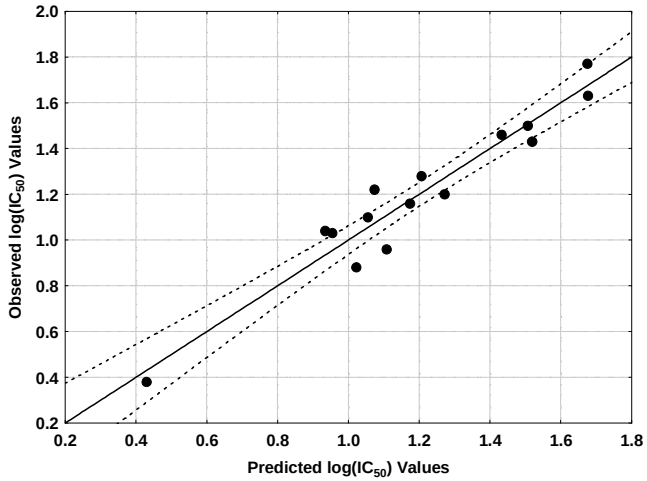

Fig. 13. Observed *vs.* calculated values (Eq. 9) of log (IC_{50}). Dashed lines denote the 95% confidence interval.

Results for the 769-P Cell Line

Group IA results

It was not possible to obtain any statistically significant equation for this set of molecules.

Group IB results

The best equation obtained is:

$$\log(IC_{50}) = 0.90 + 13.91F_7(HOMO-2)^* - 1.61F_{16}(HOMO)^* - 1.63F_{17}(LUMO)^* - \\ -0.80S_4^E(HOMO-2)^* \quad (10)$$

with n=18, R=0.96, R^2=0.92, adj-R^2=0.90, F(4,13)=38.51 (p<0.000001) and SD=0.11. No outliers were detected and no residuals fall outside the ±2σ limits. Here, $F_7(HOMO-2)^*$ is the Fukui index of the third highest occupied MO localized on atom 7, $F_{16}(HOMO)^*$ is the Fukui index of the highest occupied MO localized on atom 16, $F_{17}(LUMO)^*$ is the Fukui index of the lowest vacant MO localized on atom 17 and $S_4^E(HOMO-2)^*$ is the electrophilic superdelocalizability of the third highest occupied MO localized on atom 4. Table 14 shows the beta coefficients and the results of the t-test for significance of coefficients. Fig. 14 displays the plot of observed *vs.* calculated log(IC_{50}) values. The associated statistical parameters of Eq. 10 indicate that this equation is statistically significant and that the variation of the numerical value of a group of four local atomic reactivity indices of atoms of the common skeleton explains about 90% of the variation of the cytotoxicity.

Table 14. Beta coefficients and *t*-test for significance of coefficients in Eq. 10.

	Beta	t(13)	p-level
$F_7(HOMO-2)^*$	0.70	8.76	<0.000001
$F_{16}(HOMO)^*$	-0.63	-7.60	<0.000004
$F_{17}(LUMO)^*$	-0.35	-4.20	<0.001
$S_4^E(HOMO-2)^*$	-0.29	-3.70	<0.003

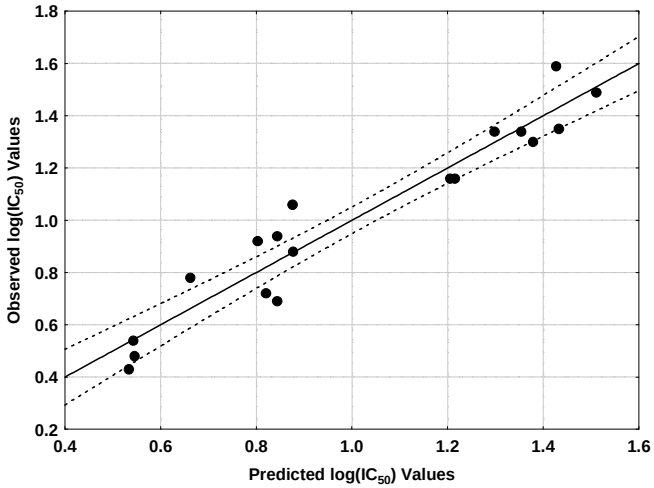

Fig. 14. Observed *vs.* calculated values (Eq. 10) of log (IC_{50}). Dashed lines denote the 95% confidence interval.

Results for the A375 Cell Line

Group IA results

The best equation obtained was:

$$\log(IC_{50}) = 4.37 - 0.001S_{10}^{N} + 0.48\mu_6 - 0.94S_{17}^{E}(HOMO-2)^* - 6.07F_{14}(LUMO+1)^* + \\ +4.52F_{16}(LUMO+2)^* \quad (11)$$

with n=13, R=0.98, R^2=0.95, adj-R^2=0.92, F(4,7)=29.64 (p<0.0001) and SD=0.10. No outliers were detected and no residuals fall outside the ±2σ limits. Here, S_{10}^{N} is the nucleophilic superdelocalizability of atom 10, μ_6 is the local atomic electronic chemical potential of atom 6, $S_{17}^{E}(HOMO-2)^*$ is the electrophilic superdelocalizability of the third highest occupied MO localized on atom 17, $F_{14}(LUMO+1)^*$ is the Fukui index of the second lowest vacant MO of atom 14 and $F_{16}(LUMO+2)^*$ is the Fukui index of the third lowest vacant MO localized on atom 16. Table 15 shows the beta coefficients and the results of the t-test for significance of coefficients. Fig. 15 displays the plot of observed *vs.* calculated log(IC_{50}) values. The associated statistical parameters of Eq. 11 indicate that this equation is statistically significant and that the variation of the numerical value of a group of five local atomic reactivity indices of atoms of the common skeleton explains about 92% of the variation of the cytotoxicity.

Table 15. Beta coefficients and *t*-test for significance of coefficients in Eq. 11.

	Beta	t(7)	p-level
S_{10}^{N}	-0.57	-5.66	<0.0008
μ_6	0.34	3.88	<0.0060
$S_{17}^{E}(HOMO-2)^*$	-0.59	-6.14	<0.0005
$F_{14}(LUMO+1)^*$	-0.40	-4.43	<0.003
$F_{16}(LUMO+2)^*$	0.35	3.44	<0.01

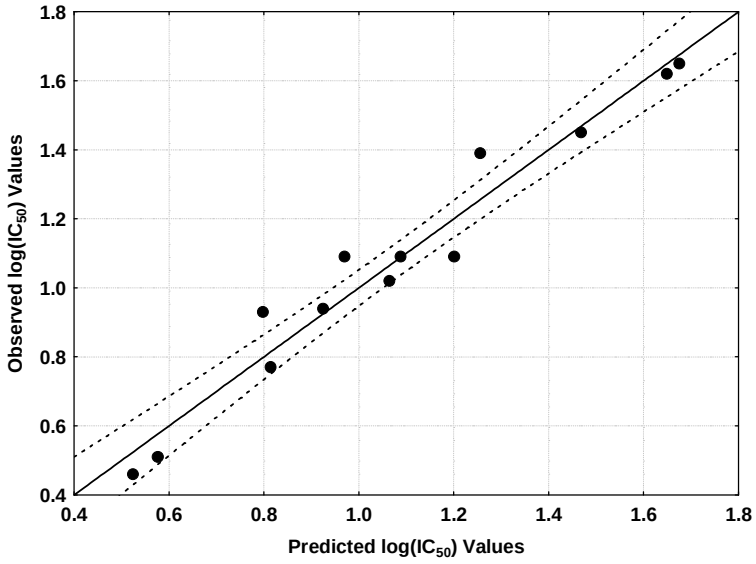

Fig. 15. Observed *vs.* calculated values (Eq. 11) of log (IC_{50}). Dashed lines denote the 95% confidence interval.

Group IB results

The best equation obtained was:

$$\log(IC_{50}) = 5.17 - 0.002S_4^N - 0.0002\phi_{R1} - 0.32\eta_{18} + 13.59Q_{16} + 0.06S_{14}^N(LUMO+2)* + \\ +0.76F_9(HOMO-1)* \quad (12)$$

with n=19, R=0.96, R^2=0.93, adj-R^2=0.89, F(6,12)=26.52 (p<0.000001) and SD=0.11. No outliers were detected and no residuals fall outside the ±2σ limits. Here, S_4^N is the nucleophilic superdelocalizability of atom 4, ϕ_{R1} is the orientational parameter of the R_1 substituent, η_{18} is the local atomic hardness of atom 18, Q_{16} is the net charge of atom 16, $S_{14}^N(LUMO+2)*$ is the nucleophilic superdelocalizability of the third lowest vacant MO localized on atom 14 and $F_9(HOMO-1)*$ is the Fukui index of the second highest occupied MO localized on atom 9. Table 16 shows the beta coefficients and the results of the t-test for significance of coefficients. Fig. 16 displays the plot of observed *vs.* calculated log(IC_{50}) values. The associated statistical parameters of Eq. 12 indicate that this equation is statistically significant and that the variation of the numerical value of a group of six local atomic reactivity indices of atoms of the common skeleton explains about 89% of the variation of the cytotoxicity.

Table 16. Beta coefficients and *t*-test for significance of coefficients in Eq. 12.

	Beta	t(12)	p-level
S_4^N	-0.53	-6.32	<0.00004
ϕ_{R1}	-0.76	-7.58	<0.00001
η_{18}	-0.33	-3.43	<0.005
Q_{16}	0.23	3.00	<0.01
$S_{14}^N(LUMO+2)*$	0.25	2.98	<0.01
$F_9(HOMO-1)*$	0.25	2.76	<0.02

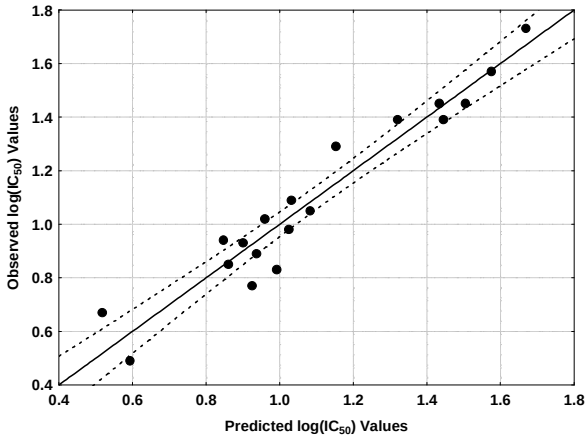

Fig. 16. Observed *vs.* calculated values (Eq. 12) of log (IC_{50}). Dashed lines denote the 95% confidence interval.

Results for the SK-OV-3 Cell Line

Group IA results

After eliminating one molecule from the set, the following equation was obtained:

$$\log(IC_{50}) = 14.42 + 0.00007\phi_{R3} - 2.16\eta_{21} + 2.42F_{22}(HOMO)* \quad (13)$$

with n=11, R=0.98, R^2=0.96, adj-R^2=0.95, F(3,7)=60.93 (p<0.00002) and SD=0.07. No outliers were detected and no residuals fall outside the ±2σ limits. Here, ϕ_{R3} is the orientational parameter of the R_3 substituent, η_{21} is the local atomic hardness of atom 21 and $F_{22}(HOMO)*$ is the Fukui index of the highest occupied MO localized on atom 22. Table 17 shows the beta coefficients and the results of the t-test for significance of coefficients. Fig. 17 displays the plot of observed *vs.* calculated log(IC_{50}) values. The associated statistical parameters of Eq. 13 indicate that this equation is statistically significant and that the variation of the numerical value of a group of three local atomic reactivity indices of atoms of the common skeleton explains about 95% of the variation of the cytotoxicity.

Table 17. Beta coefficients and *t*-test for significance of coefficients in Eq. 13.

	Beta	t(7)	p-level
ϕ_{R3}	0.52	6.47	<0.0003
η_{21}	-0.67	-7.77	<0.0001
$F_{22}(HOMO)*$	0.33	4.22	<0.004

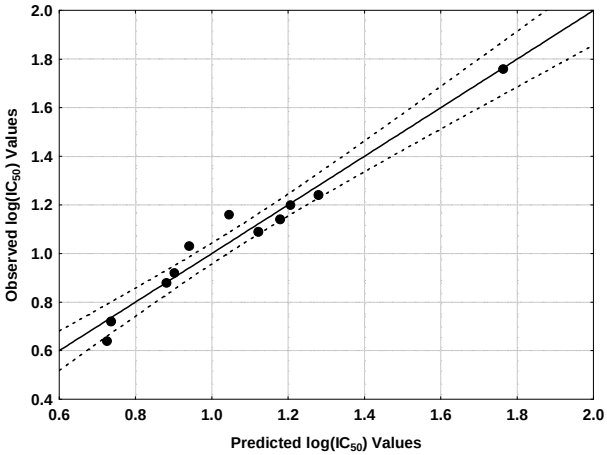

Fig. 17. Observed *vs.* calculated values (Eq. 13) of log (IC_{50}). Dashed lines denote the 95% confidence interval.

Group IB results

The best equation was:

$$\log(IC_{50}) = 8.33 - 0.0007S_{11}^{N} - 0.34S_{18}^{E}(HOMO-1)^{*} - 0.0001\phi_{R1} + \\ +0.92F_{3}(HOMO-1)^{*} - 27.40Q_{8} \quad (14)$$

with n=19, R=0.95, R^2=0.90, adj-R^2=0.86, F(5,13)=23.74 (p<0.000001) and SD=0.12. No outliers were detected and no residuals fall outside the ±2σ limits. Here, S_{11}^{N} is the nucleophilic superdelocalizability of atom 11, $S_{18}^{E}(HOMO-1)^{*}$ is the electrophilic superdelocalizability of the second highest occupied MO localized on atom 18, ϕ_{R1} is the orientational parameter of the R_1 substituent, $F_3(HOMO-1)^{*}$ is the Fukui index of the second highest occupied MO localized on atom 3 and Q_8 is the net charge of atom 8. Table 18 shows the beta coefficients and the results of the t-test for significance of coefficients. Fig. 18 displays the plot of observed *vs.* calculated log(IC_{50}) values. The associated statistical parameters of Eq. 14 indicate that this equation is statistically significant and that the variation of the numerical value of a group of five local atomic reactivity indices of atoms of the common skeleton explains about 86% of the variation of the cytotoxicity.

Table 18. Beta coefficients and *t*-test for significance of coefficients in Eq. 14.

	Beta	t(13)	p-level
S_{11}^{N}	-0.41	-4.22	<0.001
$S_{18}^{E}(HOMO-1)^{*}$	-0.58	-6.26	<0.00003
ϕ_{R1}	-0.68	-5.69	<0.00007
$F_3(HOMO-1)^{*}$	0.29	3.08	<0.009
Q_8	-0.32	-2.75	<0.02

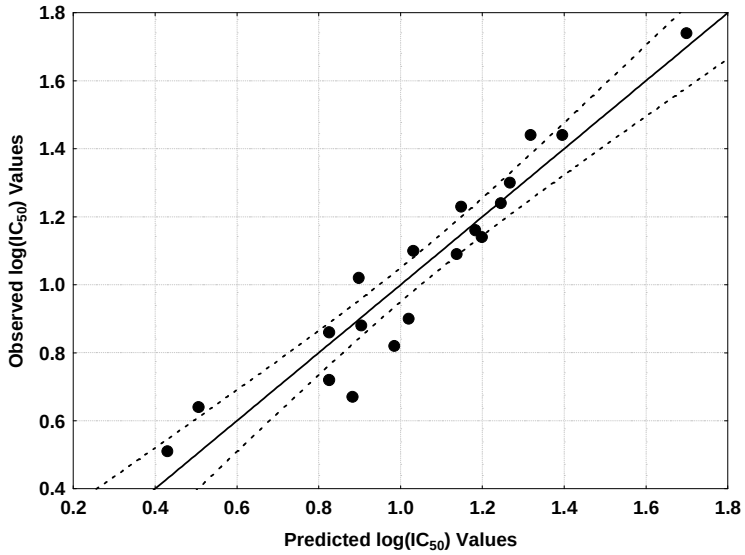

Fig. 18. Observed *vs.* calculated values (Eq. 14) of log (IC_{50}). Dashed lines denote the 95% confidence interval.

Results for the Eca-109 Cell Line
Group IA results

$$\log(IC_{50}) = -11.55 + 58.56F_8(LUMO+2)^* + 6.63S_{10}^N(LUMO)^* + 3.53F_{16}(HOMO-1)^* + \\ +31.42F_{11}(LUMO)^* \quad (15)$$

with n=16, R=0.96, R^2=0.93, adj-R^2=0.90, F(4,11)=36.09 (p<0.000001) and SD=0.13. No outliers were detected and no residuals fall outside the ±2σ limits. Here, $F_8(LUMO+2)^*$ is the Fukui index of the third lowest vacant MO localized on atom 8, $S_{10}^N(LUMO)^*$ is the nucleophilic superdelocalizability of the lowest vacant MO localized on atom 10, $F_{16}(HOMO-1)^*$ if the Fukui index of the second highest occupied MO localized on atom 16 and $F_{11}(LUMO)^*$ is the Fukui index of the lowest vacant MO localized on atom 11. Table 19 shows the beta coefficients and the results of the t-test for significance of coefficients. Fig. 19 displays the plot of observed *vs.* calculated log(IC_{50}) values. The associated statistical parameters of Eq. 15 indicate that this equation is statistically significant and that the variation of the numerical value of a group of four local atomic reactivity indices of atoms of the common skeleton explains about 90% of the variation of the cytotoxicity.

Table 19. Beta coefficients and *t*-test for significance of coefficients in Eq. 15.

	Beta	t(11)	p-level
$F_8(LUMO+2)^*$	0.87	9.48	<0.000001
$S_{10}^N(LUMO)^*$	0.63	7.45	<0.00001
$F_{16}(HOMO-1)^*$	0.79	7.39	<0.00001
$F_{11}(LUMO)^*$	0.47	4.76	<0.0006

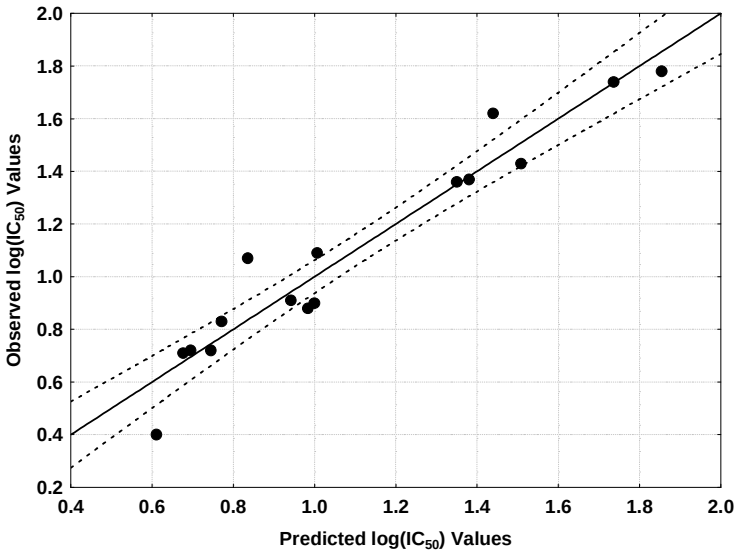

Fig. 19. Observed *vs.* calculated values (Eq. 15) of log (IC_{50}). Dashed lines denote the 95% confidence interval.

Group IB results
No statistically significant equation was obtained for this group.

Results for the BGC-823 Cell Line
Group IA results
The best equation obtained was:

$$\log(IC_{50}) = 140.21 + 1422.74Q_2 - 1.71S_{16}^{E}(HOMO-1)^* + 19.53F_{16}(LUMO+1)^* - \\ -0.66\eta_8 \quad (16)$$

with n=16, R=0.96, R^2=0.93, adj-R^2=0.90, F(4,11)=36.09 (p<0.000001) and SD=0.13. No outliers were detected and no residuals fall outside the ±2σ limits. Here, Q_2 is the net charge of atom 2, $S_{16}^{E}(HOMO-1)^*$ is the electrophilic superdelocalizability of the second highest occupied MO localized on atom 16, $F_{16}(LUMO+1)^*$ is the Fukui index of the second lowest vacant MO localized on atom 16 and η_8 is the local atomic hardness of atom 8. Table 20 shows the beta coefficients and the results of the t-test for significance of coefficients. Fig. 20 displays the plot of observed *vs.* calculated log(IC_{50}) values. The associated statistical parameters of Eq. 16 indicate that this equation is statistically significant and that the variation of the numerical value of a group of four local atomic reactivity indices of atoms of the common skeleton explains about 90% of the variation of the cytotoxicity.

Table 20. Beta coefficients and *t*-test for significance of coefficients in Eq. 16.

	Beta	t(10)	p-level
Q_2	1.19	9.79	<0.000002
$S_{16}^{E}(HOMO-1)^*$	-0.80	-6.21	<0.0001
$F_{16}(LUMO+1)^*$	0.54	4.34	<0.001
η_8	-0.27	-2.44	<0.03

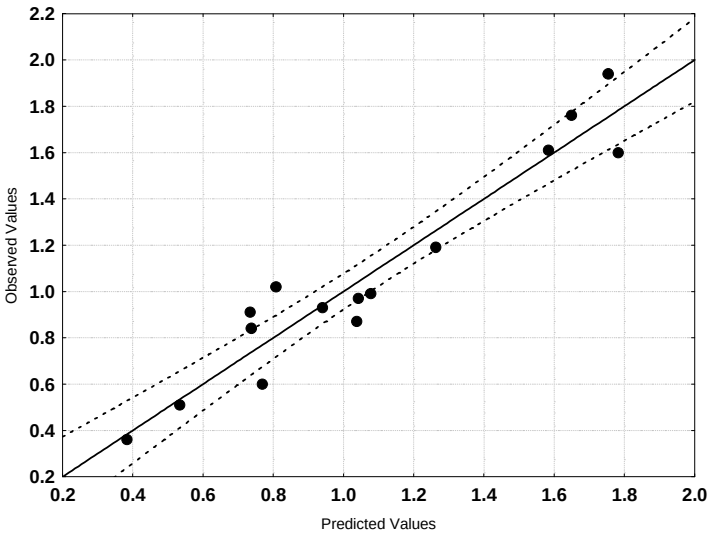

Fig. 20. Observed *vs.* calculated values (Eq. 16) of log (IC_{50}). Dashed lines denote the 95% confidence interval.

Group IB results
The best equation obtained is:

$$\log(IC_{50}) = 21.11 - 0.0001\phi_{R1} + 30.72s_{17} + 186.01Q_4 - 17.15s_{10} - 1.28F_{16}(HOMO)^* \quad (17)$$

with n=17, R=0.94, R^2=0.88, adj-R^2=0.82, F(5,11)=15.59 (p<0.0001) and SD=0.20. No outliers were detected and no residuals fall outside the ±2σ limits. Here, ϕ_{R1} is the orientational parameter of the R_1 substituent, s_{17} is the local atomic softness of atom 17, Q_4 is the net charge of atom 4, s_{10} is the local atomic softness of atom 10 and

$F_{16}(HOMO)*$ is the Fukui index of the highest occupied MO localized on atom 16. Table 21 shows the beta coefficients and the results of the t-test for significance of coefficients. Fig. 21 displays the plot of observed *vs.* calculated log(IC_{50}) values. The associated statistical parameters of Eq. 17 indicate that this equation is statistically significant and that the variation of the numerical value of a group of five local atomic reactivity indices of atoms of the common skeleton explains about 82% of the variation of the cytotoxicity.

Table 21. Beta coefficients and *t*-test for significance of coefficients in Eq. 17.

	Beta	t(11)	p-level
ϕ_{R1}	-0.48	-3.79	<0.003
s_{17}	0.55	4.74	<0.001
Q_4	0.54	3.86	<0.003
s_{10}	-0.30	-2.73	<0.019
$F_{16}(HOMO)*$	-0.36	-2.43	<0.033

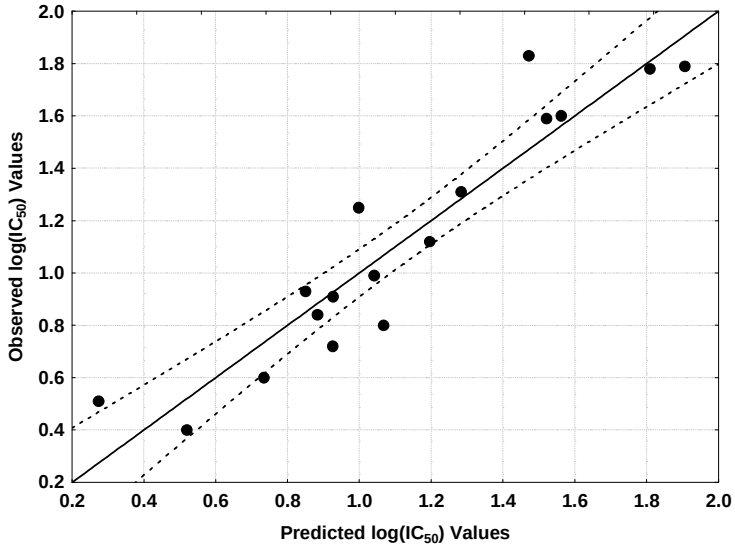

Fig. 21. Observed *vs.* calculated values (Eq. 17) of log (IC_{50}). Dashed lines denote the 95% confidence interval.

DISCUSSION

Molecular Electrostatic Potential (MEP)

As all the molecules are in their cationic form, they are surrounded by a positive MEP. Figures 22 and 23 show, respectively, the MEP distribution of molecule 21 at 4.5 Å of the nuclei and at an isovalue of 0.02 [106, 107].

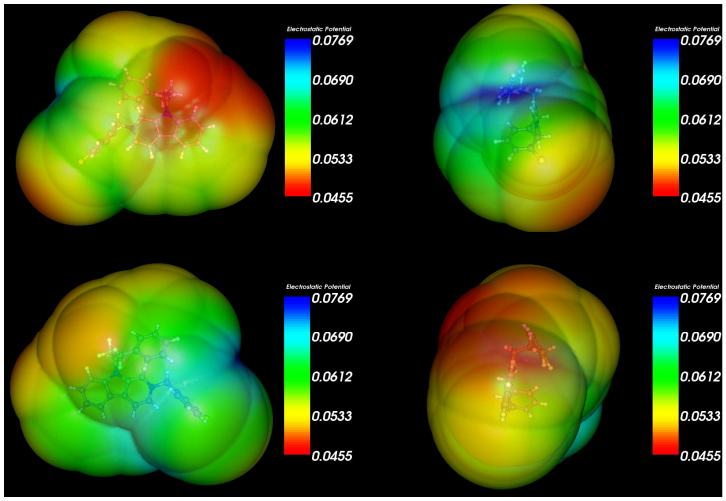

Figure 22. MEP map of molecule 21 at 4.5Å of the nuclei. The upper left figure was rotated 90° to show the entire surface.

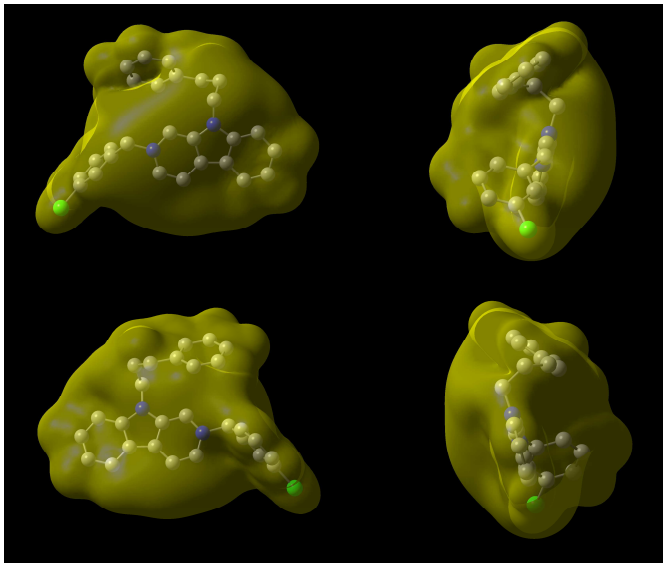

Figure 23. MEP map of molecule 21 at an isovalue of 0.02. The upper left figure was rotated 90° to show the entire surface.

This kind of MEP distribution is characteristic of molecules possessing a positive net charge. It is not possible to build any relationship between MEP and cytoxicity but it is possible to suggest that in the active site there should be negatively charged residues (carboxylate) or negative ions to neutralize the molecule's MEP.

Conformational flexibility

In the case of group IA the chain joining N9 with ring D allows a high degree of conformational flexibility. For group IB ring D has less conformational flexibility since it is connected to ring B only by a CH_2 group. We do not know the real conformation of these molecules in the moment when they exert their biological action (see below). As examples of this conformational flexibility we show in Fig. 24 the superimposition of the ten lowest energy conformers of molecules 1, 13, 23 (this molecule has a $(CH_2)_2$ linker between rings C and D) and 24 (this molecule has a $(CH_2)_3$ linker between rings C and D). They were calculated with MarvinView software and with the Dreiding Force Field. The superimposition process was carried out with Hyperchem [108, 109].

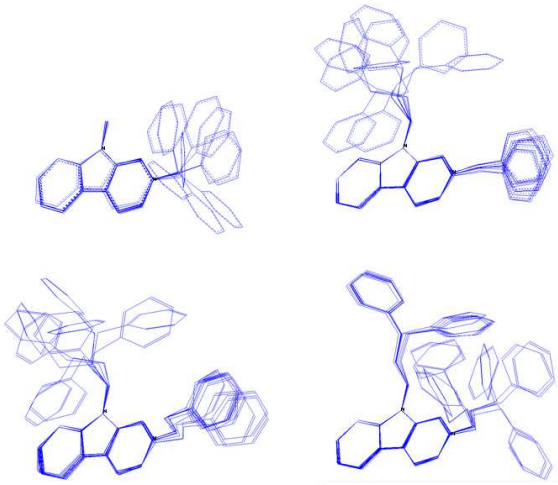

Figure 24. Superimposition of the ten lowest energy conformers of molecules 1 (upper left), 13 (upper right), 23 (lower left) and 24 (lower right).

Despite the fact that ring D can adopt several conformations in groups IA and IB, in the LRMA analysis we have worked with the hypothesis that these rings adopt a very similar position at the interaction site. The results shown below strongly indicate that this idea seems to be true.

QSAR results

In all the ensuing discussions we shall employ the variable-by-variable analysis. This approach provides a good insight on the main molecular-electronic factors involved in the biological process. In the ensuing discussion the concept of "local molecular orbital" will be employed. For atom i, the set of its local molecular orbitals is formed by those MO localized on it. For example, $(HOMO-2)_{11}$* refers to the third highest occupied MO localized on atom 11. Tables 22 to 25 show the local MO structure for several atoms belonging to group IA. The nomenclature is: Molecule (HOMO) / (HOMO-2)* (HOMO-1)* (HOMO)* - (LUMO)* (LUMO+1)* (LUMO+2)*.

Table 22. Local MO structure of atoms 6 to 8 of group IA.

Mol.	Atom 6	Atom 7	Atom 8
13(100)	96π97π98π-102π105π106π	94π97π98π-101π102π105π	95π96π97π-101π102π105π
14(80)	76π77π78π-82π83π84π	76π77π78π-81π82π83π	74π76π77π-81π82π83π
15(84)	80π81π84π-86π87π90π	80π81π84π-85π86π87π	76π80π81π-85π86π87π
16(92)	88π89π92π-94π95π98π	88π89π92π-93π94π95π	83π88π89π-93π94π95π
17(100)	96π97π100π-101π102π103π	96π97π100π-101π102π103π	88π96π97π-101π102π103π
18(108)	104π105π108π-109π110π111π	101π105π108π-109π110π111π	94π101π105π-109π110π111π
19(116)	112π113π116π-117π118π119π	112π113π116π -117π118π119π	108π112π113π-117π118π119π
20(104)	100π102π104π-105π106π109π	98π100π104π-105π106π109π	98π100π102π-105π106π109π
21(108)	102π104π108π-109π110π113π	102π104π108π-109π110π113π	99π102π104π-109π110π113π
22(111)	105π108π111π-114π116π120π	102π108π111π-112π114π116π	98π102π108π-112π114π115π
23(104)	98π99π104π-105π106π107π	99π102π104π-105π106π107π	92π98π99π-105π106π107π
24(108)	102π103π107π-109π110π111π	103π105π107π-109π110π111π	96π102π103π-109π110π111π
25(104)	101π102π103π-105π106π108π	102π103π104π-105π106π109π	98π 99π101π-105π106π107π
26(120)	116π119π120π-121π122π123π	115π119π120π-121π122π126π	113σ115π116π-121π122π123σ
27(128)	124π126π128π-129π130π131π	122π126π128π-129π130π134π	122π123π128π-129π130π131π
28(121)	117π120π121π-122π123π124π	113π120π121π-122π123π126π	115π116π117π-122π123π124π

Table 23. Local MO structure of atoms 9-11 of group IA.

Mol.	Atom 9	Atom 10	Atom 11
13(100)	94π98π100π -101π102π105π	94π97π98π-101π102π105π	95σ97π98π-101π102π103σ
14(80)	76π78π80π-81π82π83π	76π77π78π-81π82π83π	76π77π78π-81π82π83π
15(84)	77π80π84π-85π86π87π	80π81π84π-85π86π87π	80π81π84π-85π86π87π
16(92)	86π88π92π-93π94π95π	88π89π92π-93π94π95π	88π89π92π-93π94π95π
17(100)	89π96π100π-101π102π103π	96π97π100π-101π102π103π	96π97π100π-101π102π103π
18(108)	95π101π108π-109π110π111π	101π105π108π-109π110π111π	101π105π108π-109π110π111π
19(116)	107π108π116π-117π118π119π	112π113π116π-117π118π119π	108π112π116π-117π118π119π
20(104)	96π98π104π-105π106π109π	98π100π104π-105π106π109π	98π100π104π-105π106π107σ
21(108)	98π102π108π-109π110π113π	102π104π108π-109π110π113π	102π104π108π-109π110π111σ
22(111)	100π102π111π-112π114π116π	102π108π111π-112π114π115π	102π108π111π-112π114π116π
23(104)	98π102π104π-105π106π107π	98π99π104π-105π106π107π	98π99π104π-105π106π107π
24(108)	102π105π107π-109π110π111π	102π103π107π-109π110π111π	102π103π107π-109π110π111π
25(104)	102π103π104π-105π106π109π	99π101π103π-105π106π109π	102π103π104π-105π106π108π
26(120)	112π119π120π-121π122π126π	115π116π119π-121π122π123π	115π119π120π-121π122π123σ
27(128)	125π126π128π-129π130π134π	123π124π128π-129π130π132π	122π126σ128π-129π130π131σ
28(121)	113π120π121π-122π123π126π	116π117π120π-122π123π124π	116π120π121π-122π123π124σ

Table 24. Local MO structure of atoms 14, 16 and 17 of group IA.

Mol.	Atom 14	Atom 16	Atom 17
13(100)	94σ98σ100σ-106σ107σ112σ	93σ94σ100σ-107σ118σ119σ	94σ98π100π-106π107π108π
14(80)	76σ78σ80σ-85σ90σ91σ	75σ76σ80σ-85σ94σ96σ	76σ78π80π-85π86π88π
15(84)	79σ80σ84σ-93σ94σ95σ	78σ79σ83σ-88σ89σ92σ	79σ82π83π-88π89π90π
16(92)	87σ88σ92σ-103σ105σ106σ	86σ87σ91σ-96σ97σ100σ	87σ90π91π-96π97π98π
17(100)	91σ96σ100σ-111σ113σ114σ	92σ98σ99σ-104σ105σ106σ	92σ98π99π-104π105π106π
18(108)	97σ101σ108σ-119σ121σ122σ	96σ97σ107σ-112σ113σ116σ	97σ106π107π-112π113π114π
19(116)	102σ107σ116σ-127σ129σ130σ	101σ102σ115σ-120σ121σ124σ	102σ114π115π-120π121π122π
20(104)	97σ98σ104σ-117σ119σ120σ	101σ102σ103σ-109σ110σ111σ	97σ101π103π-110π111π112π
21(108)	99σ102σ108σ-121σ122σ123σ	98σ99σ107σ-114σ119σ130σ	99σ105π107π-114π115π116π
22(111)	101σ102σ111σ-117σ125σ127σ	100σ101σ110σ-117σ122σ133σ	101σ109π110π-117π118π119π
23(104)	97σ98σ104σ-116σ117σ119σ	96σ97σ103σ-114σ120σ123σ	97σ100π103π-108π109π110π
24(108)	99σ102σ107σ-120σ121σ122σ	98σ99σ106σ-112σ113σ118σ	104π105π106π-112π113π114π
25(104)	97σ98σ104σ-110σ114σ116σ	96σ97σ104σ-111σ115σ121σ	102π103π104π-111π112π123σ
26(120)	113σ114σ120σ-128σ133σ136σ	110σ111σ120σ-128σ129σ137σ	111σ119π120π-128π129π130π
27(128)	120σ126σ128σ-136σ141σ144σ	118σ119σ127σ-136σ137σ146σ	126π127π128π-136π137π138π
28(121)	113σ114σ121σ-128σ135σ136σ	111σ112σ121σ-128σ129σ134σ	112σ120π121π-128π129π130π

Table 25. Local MO structure of atoms 18, 19 and 22 of group IA.

Mol.	Atom 18	Atom 19	Atom 22
13(100)	93σ99π100π-107π108π118σ	93σ99π100π-107π108π118σ	94σ99π100π-107π108π122π
14(80)	76σ79π80π-85π86π96σ	76σ79π80π-85π86π96σ	76σ79π80π-85π86π96σ
15(84)	79σ82π83π-88π89π97σ	79σ82π83π-88π89π97σ	79σ82π83π-87π88π89π
16(92)	87σ90π91π-95π96π97π	87σ90π91π-95π96π97π	87σ90π91π-95π96π97π
17(100)	92σ98π99π-103π104π105π	92σ98π99π-103π104π105π	92σ98π99π-103π104π105π
18(108)	97σ106π107π-111π112π113π	97σ106π107π-111π112π113π	97σ106π107π-111π112π113π
19(116)	102σ114π115π-119π120π121π	102σ114π115π-119π120π121π	102σ114π115π-119π120π121π
20(104)	101π102π103π-109π110π111π	101π102π103π-109π110π111π	101π102π103π-107π109π110π
21(108)	99σ105π107π-112π113π114π	99σ105π107π-112π113π114π	99σ105π107π-112π113π114π
22(111)	101σ109π110π-116π117π118π	101σ109π110π-116π117π118π	101σ109π110π-115π116π117π
23(104)	97σ100π103π-108π109π110π	97σ100π103π-108π109π110π	97σ100π103π-108π109π110π
24(108)	99σ104π106π-112π113π124σ	99σ104π106π-112π113π124σ	99σ104π106π-112π113π114π
25(104)	102π103π104π-111π112π124σ	102π103π104π-111π112π124σ	102π103π104π-110π111π112π
26(120)	118π119π120π-128π129π130π	118π119π120π-128π129π130π	118π119π120π-128π129π130π
27(128)	126π127π128π-136π137π138π	126π127π128π-136π137π138π	125π126π127π-136π137π138π
28(121)	119π120π121π-128π129π130π	119π120π121π-128π129π130π	119π120π121π-128π129π130π

Tables 26-28 show the local MO structure for several atoms belonging to group IB.

Table 26. Local MO structure of atoms 3, 4 and 7 of group IB.

Mol.	Atom 3	Atom 4	Atom 7
1(72)	69π70π71π-73π77π78π	70π71π72π-73π74π77π	68π71π72π-73π74π77π
2(76)	73π74π75π-77π81π82π	74π75π76π-77π78π81π	72π75π76π-77π78π81π
3(80)	77π78π79π-81π85π86π	76π79π80π-81π82π85π	76π79π80π-81π82π85π
4(79)	76π77π78π-80π84π85π	77π78π79π-80π81π84π	74π78π79π-80π81π84π
5(84)	81π82π83π-85π89π90π	82π83π84π-85π86π89π	80π83π84π-85π86π89π
6(84)	81π82π83π-85π89π90π	82π83π84π-85π86π89π	80π83π84π-85π86π89π
7(92)	89π90π91π-93π97π98π	90π91π92π-93π94π97π	88π91π92π-93π94π97π
8(100)	97π98π99π-101π105π106π	98π99π100π-101π102π105π	93π99π100π-101π102π105π
9(92)	87π88π89π-93π94π96π	89π91π92π-93π94π96π	89π91π92π-93π94π100π
10(96)	92π93π94π-97π98π101π	94π95π96π-97π98π101π	94π95π96π-97π98π101π
11(100)	95π97π98π-101π105π106π	98π99π100π-101π102π105π	97π99π100π-101π102π105π
12(100)	95π96π97π-101π102π105π	97π98π99π-101π102π105π	94π97π99π-101π102π105π
13(100)	95π96π97π-101π105π106π	96π97π98π-101π102π105π	94π97π98π-101π102π105π
20(104)	95π100π102π-105π109π112π	98π100π104π-105π106π109π	98π100π104π-105π106π109π
21(108)	96π97π104π-109π113π116π	102π104π108π-109π110π113π	102π104π108π-109π110π113π
22(111)	98π99π108π-112π116π120π	105π108π111π-112π114π116π	102π108π111π-112π114π116π
25(104)	95π99π101π-105π108π109π	102π103π104π-105π106π108π	102π103π104π-105π106π109π
26(120)	114π115π116π-121π123π125π	117π119π120π-121π122π123π	115π119π120π-121π122π126π
27(128)	122π123π124π-129π131π132π	124π126π128π-129π130π131π	122π126π128π-129π130π134π
28(121)	115π116π117π-122π124π125π	117π120π121π-122π123π125π	113π120π121π-122π123π126π

Table 27. Local MO structure of atoms 9, 14 and 16 of group IB.

Mol.	Atom 9	Atom 14	Atom 16
1(72)	67π68π72π-73π74π77π	66σ67σ69σ-75σ79σ80σ	69π70π71π-74π75π76π
2(76)	71π72π76π-77π78π81π	70σ71σ73σ-79σ83σ84σ	73π74π75π-78π79π80π
3(80)	75π76π80π-81π82π85π	74σ75σ77σ-82σ83σ87σ	74σ77π78π-82π83π84π
4(79)	74π75π79π-80π81π84π	72σ73σ76σ-82σ87σ89σ	76π77π78π-81π82π83π
5(84)	78π80π84π-85π86π89π	75σ76σ81σ-87σ91σ92σ	81π82π83π-86π87π88π
6(84)	79π80π84π-85π86π89π	75σ76σ81σ-87σ91σ92σ	75σ81π82π-86π87π88π
7(92)	86π88π92π-93π94π97π	82σ83σ89σ-95σ99σ100σ	81σ89π90π-94π95π96π
8(100)	89π93π100π-101π102π105π	88σ89σ97σ-103σ107σ108σ	85σ97π98π-102π103π104π
9(92)	86π91π92π-93π94π97π	83σ85σ87σ-95σ101σ103σ	87π88π89π-94π95π96π
10(96)	90π95π96π-97π98π101π	88σ89σ93σ-99σ105σ107σ	92π93π94π-98π99π100π
11(100)	97π99π100π-101π102π104π	90σ91σ97σ-103σ110σ112σ	96π97π98π-102π103π106π
12(100)	94π99π100π-101π102π105π	91σ95σ97σ-103σ109σ111σ	90σ95π96π-102π103π104π
13(100)	94π98π100π-101π102π105π	88σ90σ95σ-103σ109σ110σ	88σ95π96π-102π103π104π
20(104)	96π98π104π-105π106π109π	94σ95σ102σ-106σ107σ108σ	99π100π102π-106π107π108π
21(108)	98π102π108π-109π110π113π	97σ100σ103σ-110σ111σ117σ	103π104π106π-110π111π112π
22(111)	100π102π111π-112π114π116π	98σ99σ105σ-113σ114σ115σ	103π105π106π-113π114π115π
25(104)	102π103π104π-105π106π109π	94σ95σ101σ-107σ113σ114σ	99π100π101π-106π107π108π
26(120)	112π119π120π-121π122π126π	109σ114σ117σ-123σ124σ125σ	115π116π117π-122π123π125π
27(128)	125π126π128π-129π130π134π	116σ117σ124σ-131σ133σ134σ	122π123π124π-131π132π133π
28(121)	113π120π121π-122π123π126π	109σ110σ115σ-125σ126σ131σ	116π117π118π-123π125π127π

MCF-7 Cell Line
Group IA

Table 6 shows that the relative importance of the reactivity indices is $F_6(LUMO)^*$ > S_{10}^N > $F_{18}(HOMO-2)^*$ > $F_8(HOMO-2)^*$ (see Fig. 4). A low cytotoxic capacity is associated with high values for $F_6(LUMO)^*$ and $F_{18}(HOMO-2)^*$ and with small values for S_{10}^N and $F_8(HOMO-2)^*$ (a low cytoxicity means a high IC_{50} value). A high value for $F_6(LUMO)^*$, a π MO in all molecules (Table 22), suggests that atom 6 is interacting with an electron-rich center. Fig. 25 shows the $(LUMO)^*_6$ of molecules 13, 20, 24 and 28 (see Fig. 4).

Table 28. Local MO structure of atoms 17-19 of group IB.

Mol.	Atom 17	Atom 18	Atom 19
1(72)	69π70π71π-75π76π79π	67σ69π71π-75π76π79π	69π70π71π-74π75π76π
2(76)	73π74π75π-79π80π83π	73π74π75π-79π80π83π	73π74π75π-78π79π80π
3(80)	77π78π79π-82π83π84π	77π78π79π-83π84π87π	74σ77π78π-82π83π84π
4(79)	76π77π78π-82π83π87π	76π77π78π-82π83π87π	73σ76π77π-81π82π83π
5(84)	81π82π83π-87π88π91π	81π82π83π-87π88π91π	76σ81π82π-86π87π88π
6(84)	81π82π83π-87π88π91π	81π82π83π-87π88π91π	76σ81π82π-86π87π88π
7(92)	89π90π91π-95π96π99π	89π90π91π-95π96π99π	81σ89π90π-94π95π96π
8(100)	97π98π99π-103π104π107π	97π98π99π-103π104π107π	85σ97π98π-102π103π104π
9(92)	88π89π90π-95π96π97π	87π88π89π-95π96π101π	87π88π89π-95π96π97π
10(96)	91π93π94π-99π100π102π	92π93π94π-99π102π105π	92π93π94π-99π100π102π
11(100)	95π96π98π-103π106π107π	96π97π98π-103π107π110π	96π97π98π-103π106π107π
12(100)	96π97π98π-103π104π106π	91σ95π97π-103π104π109π	91σ95π96π-102π103π104π
13(100)	95π96π97π-103π104π109π	95π96π97π-103π104π109π	90σ95π96π-102π103π104π
20(104)	99π101π102π-107π108π110π	100π101π102π-107π108π113σ	99π100π102π-106π107π108π
21(108)	100π101σ106π-111π112π114π	101σ103π106π-111π112π117σ	101σ103π106π-110π111π112π
22(111)	105π106π107π-113π114π115π	104σ105π106π-113π115π117π	105π106π107π-113π114π115π
25(104)	99π100π101π-107π108π109π	99π100π101π-106π107π108π	99π100π101π-107π108π109π
26(120)	115π116π117π-124π125π126π	115π116π117π-122π123π124π	115π116π117π-123π124π125π
27(128)	122π123π124π-130π131π133π	122π123π124π-130π131π133π	122π123π124π-132π134π135π
28(121)	110σ116π117π-124π125π126π	116π117π118π-123π125π126π	117π118π119π-124π125π126π

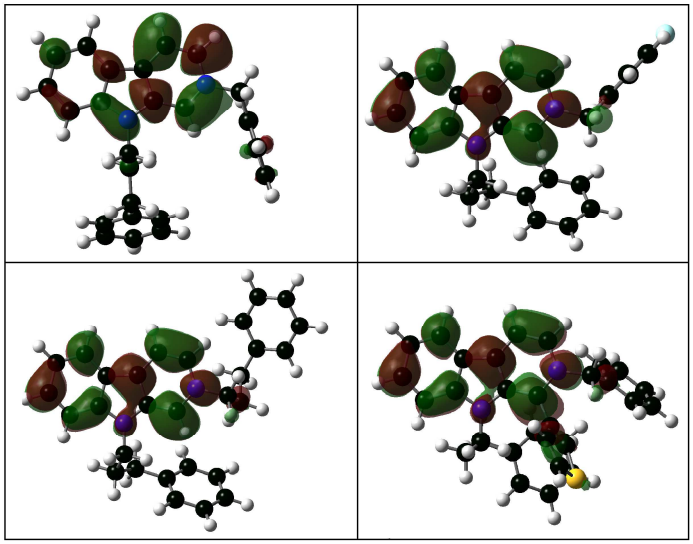

Figure 25. $(LUMO)^*_6$ **of molecules 13 (upper left), 20 (upper right), 24 (lower left) and 28 (lower right).**

A high value for $F_{18}(HOMO-2)^*$, a π or σ MO (Table 24 and Fig. 26), suggests the possible interaction of the three highest occupied MOs localized on atom 18 with an electron-deficient center. The optimal situation is a $(HOMO-2)^*_{18}$ of π nature.

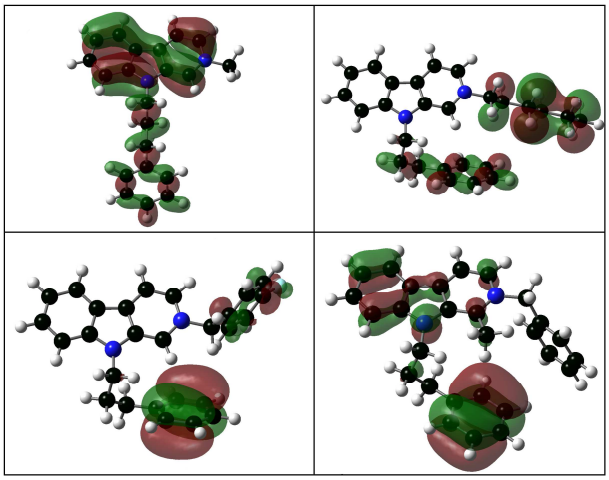

Figure 26. $(HOMO-2)^{*}_{18}$ of molecules 14 (upper left), 17 (upper right), 20 (lower left) and 25 (lower right).

A low value for S^{N}_{10} indicates that atom 10 should act as a bad electron acceptor. This could imply that atom 8 is interacting with an electron-deficient center. $F_8(HOMO-2)*$ will not be discussed because of its high p value (see Table 6). These ideas are encompassed in the two dimensional (2D) partial pharmacophore shown in Fig. 27.

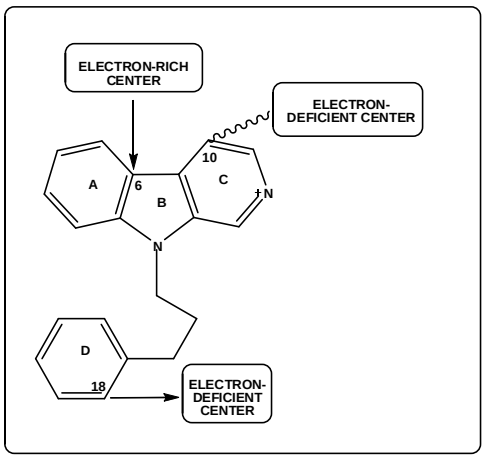

Figure 27. Partial 2D pharmacophore from Eq. 2.

Group IB

Beta values (Table 7 and Fig. 5) indicate that the relative importance of the reactivity indices is $S^{N}_{4}(LUMO)* > \phi_{R1} > F_{14}(LUMO)* = S^{N}_{18}(LUMO+1)* > Q^{\max}_{9}$. A low cytotoxic capacity is associated with high values for $S^{N}_{4}(LUMO)*$, $Q^{\max}_{9}$ and $S^{N}_{18}(LUMO+1)*$; and with low values for $F_{14}(LUMO)*$ and ϕ_{R1}. A high value for $S^{N}_{4}(LUMO)*$, a π MO in all molecules (Table 26), indicates that atom 4 interacts with an electron-rich area. Figure 28 displays the $(LUMO)^{*}_{4}$ of molecules 3, 8, 12 and 27.

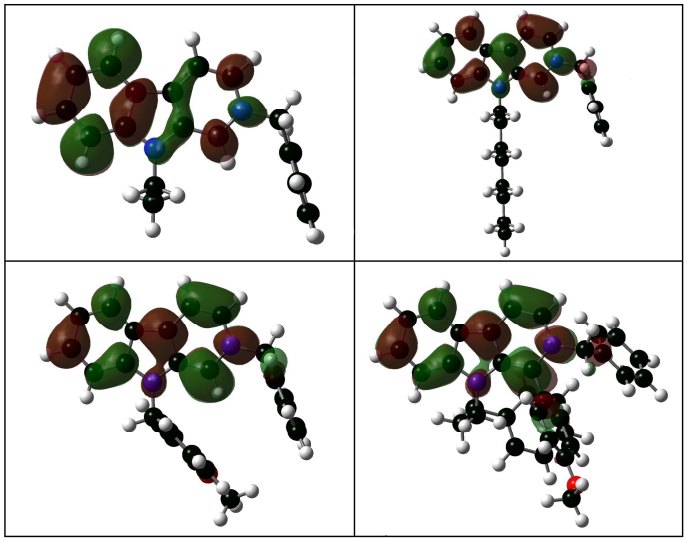

Figure 28. $(LUMO)^*_4$ **of molecules 3 (upper left), 8 (upper right), 12 (lower left) and 27 (lower right).**

Q_9^{max} will not be discussed because of its high p value (see Table 7). $(LUMO+1)^*_{18}$ and $(LUMO)^*_{18}$ are of π nature in all molecules (Table 28). As a high value of $(LUMO+1)^*_{18}$ is associated with low toxicity, we propose that atom 18 is interacting with an electron-rich center through its two lowest vacant MOs. Atom 14, a carbon from a CH_2 group, has only σ MOs. As a low value is required for $F_{14}(LUMO)^*$, it is proposed that this atom is interacting with one or more empty σ MOs from a residue of the site. A low value for ϕ_{R1} suggests that in some cases molecules are less cytotoxic when R_1 is a methyl or an ethyl group. An important implication of this fact is that ring D seems to be an extra site for binding (see Fig. 3 and Table 5). These suggestions are resumed in the partial 2D pharmacophore shown in Fig. 29.

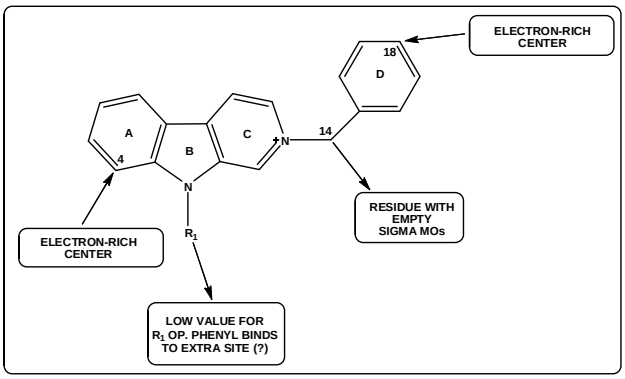

Figure 29. Partial 2D pharmacophore from Eq. 3.

HepG2 Cell Line
Group IA

Beta values (Table 8) indicate that the relative importance of the reactivity indices is $S_7^N(LUMO)^* > F_{16}(HOMO-1)^* > \phi_{R2} > S_8^N(LUMO+2)^* > S_{19}^N(LUMO)^*$ (Fig. 4). A VbV analysis shows that a low cytotoxicity is related to high values for $F_{16}(HOMO-1)^*$ and $S_8^N(LUMO+2)^*$; and with low values

for $S_7^N(LUMO)^*$, ϕ_{R2} and $S_{19}^N(LUMO)^*$. A high value for $F_{16}(HOMO-1)^*$, a σ OM in all molecules (Table 24), suggests that atom 16 is interacting with a region with empty σ MOs through its first two highest occupied MOs. Fig. 30 shows, as an example, the $(HOMO\text{-}1)_{16}^*$ of molecules 14, 18, 23 and 26.

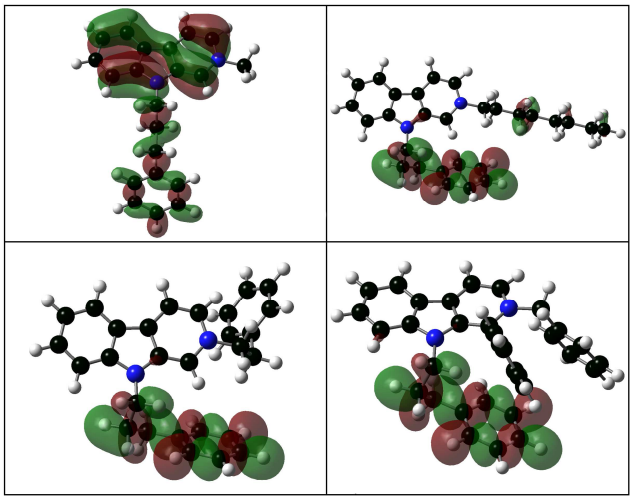

Figure 30. $(HOMO-1)_{16}^*$ **of molecules 14 (upper left), 18 (upper right), 23 (lower left) and 26 (lower right).**

A high value for $S_8^N(LUMO+2)^*$, a π MO in almost all molecules (Table 22), strongly suggests that atom 8 is interacting with an electron-rich center through its first three lowest vacant MOs. A low value for $S_7^N(LUMO)^*$, a negative number in all molecules, is obtained by shifting downwards the energy of the associated eigenvalue. This implies that atom 7 seems to interact with an electron-rich center. A low value for ϕ_{R2} suggests that the R_2 substituent should be small (methyl, ethyl). This implies that a CH_2-phenyl moiety is not absolutely necessary for activity and that it is interacting with an extra site. A low value for $S_{19}^N(LUMO)^*$, a negative number, indicates that atom 19 is interacting with an electron-rich center. These suggestions are shown in the partial 2D pharmacophore shown in Fig. 31.

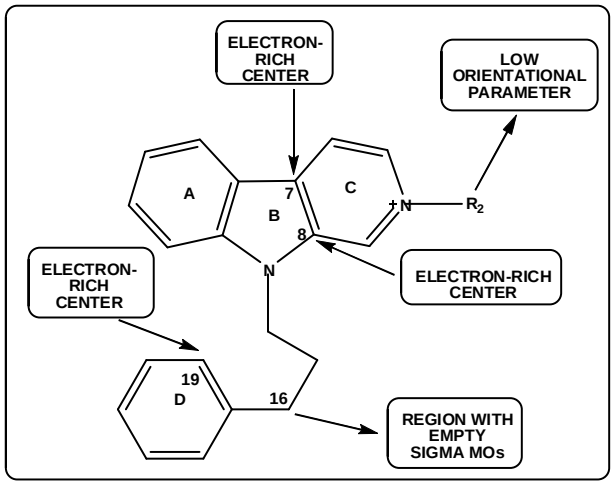

Figure 31. Partial 2D pharmacophore from Eq. 4.

Group IB

Beta values (Table 9 and Fig. 5) indicate that the relative importance of the variables is ϕ_{R1} > $S_9^N(LUMO)*$ > η_{18} > $F_4(HOMO-2)*$. A VbV analysis shows that a low cytoxicity is associated with high values for $F_4(HOMO-2)*$ and with low values for ϕ_{R1}, $S_9^N(LUMO)*$ and η_{18}. $(HOMO\text{-}2)_4^*$ is a π MO (Table 26). A high value for $F_4(HOMO-2)*$ suggests that atom 4 interacts with an electron-deficient site through its three highest occupied MOs (Table 26). For a low value for ϕ_{R1}, substituents such as methyl, ethyl and the several isomers for C_nH_{n-1} should be explored. They will not alter appreciably the electronic structure of the A-C ring system. $(LUMO)_9^*$ is a π MO is all molecules (Table 27). A low value for $S_9^N(LUMO)*$ suggests that this atom should behave as a good electron-acceptor (this index has negative numerical values) and probably it is interacting with a rich-electron moiety. A low numerical value for η_{18}, the $(HOMO)_{18}^*$-$(LUMO)_{18}^*$ distance, can be obtained by shifting downwards the energy of $(LUMO)_{18}^*$. Therefore, it is suggested that atom 18 interacts with a rich-electron counterpart. These suggestions are shown in the partial 2D pharmacophore shown in Fig. 32.

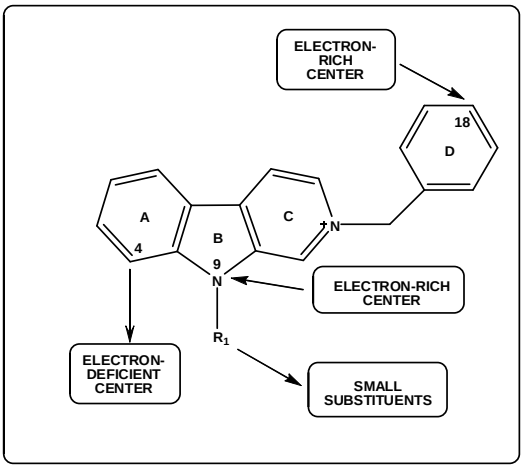

Figure 32. Partial 2D pharmacophore from Eq. 5.

22RV1 Cell Line
Group IA

Beta values (Table 10 and Fig. 4) indicate that the relative importance of the variables is $S_9^N(LUMO)*$ > s_{18} > $S_{11}^E(HOMO-2)*$ > $F_{17}(HOMO-2)*$. A VbV analysis shows that a low cytoxicity is associated with high values for $F_{17}(HOMO-2)*$ and s_{18}; and with low values for $S_9^N(LUMO)*$ and $S_{11}^E(HOMO-2)*$. The case of $F_{17}(HOMO-2)*$ deserves a comment. $(HOMO-2)_{17}^*$ is a σ MO, while the two highest occupied MOs are of π character (Table 24). A tentative interpretation for a high numerical value for this index is that atom 17 is interacting with an electron-deficient center possessing one or two vacant π followed by vacant σ MOs or that this atom is interacting with one site with empty π MOs and with another with σ empty MOs. We have not enough data to carry out a deeper analysis. A high value for s_{18} is obtained by diminishing the $(HOMO)_{18}^*$-$(LUMO)_{18}^*$ distance, making atom 18 a good electron acceptor. It is suggested then that this atom interacts with an electron-rich center. A small value for $S_9^N(LUMO)*$ (with negative numerical values and π nature, Table 23) indicates that this atom is also interacting with an electron-rich center. A small value for $S_{11}^E(HOMO-2)*$ ($(HOMO-2)_{11}^*$ is a π or σ MO, Table 23) is obtained by shifting downwards the MO energy. It is possible that atom 11 interacts

with an electron-deficient center having empty π MOs and occupied σ MOs. These ideas are shown in the partial 2D pharmacophore shown in Fig. 33.

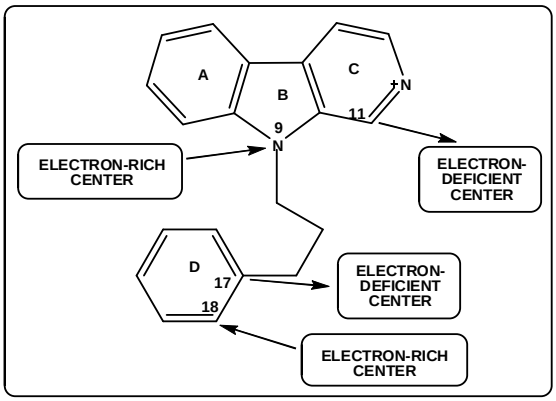

Figure 33. Partial 2D pharmacophore from Eq. 6.

Group IB

Beta values (Table 11 and Fig. 5) indicate that the relative importance of the variables is $S_9^N(LUMO)^* > \eta_{19} > S_4^N(LUMO+2)^* > \phi_{R1} > F_{19}(HOMO-2)^*$. A VbV analysis shows that a low cytoxicity is associated with low values for all these indices. A low value for $S_9^N(LUMO)^*$ (a negative number) indicates that atom 9 is interacting with an electron-rich center through its $(HOMO)_9^*$, a π MO (Table 27). A low numerical value for η_{19} is an indication that atom 19 is also interacting with an electron-rich center. $(LUMO+2)_4^*$ is a π MO (Table 26). A low value for $S_4^N(LUMO+2)^*$ could be an indication that atom 4 interacts with an electron-rich center only through its two lowest vacant MOs. A low value for ϕ_{R1} suggest that small alkyl substituents will be optimal for low cytoxicity but we must not forget that there is a possibility of an extra interaction with the site through ring D. $F_{19}(HOMO-2)^*$ will not be discussed because of its high p value. These ideas are shown in the partial 2D pharmacophore shown in Fig. 34.

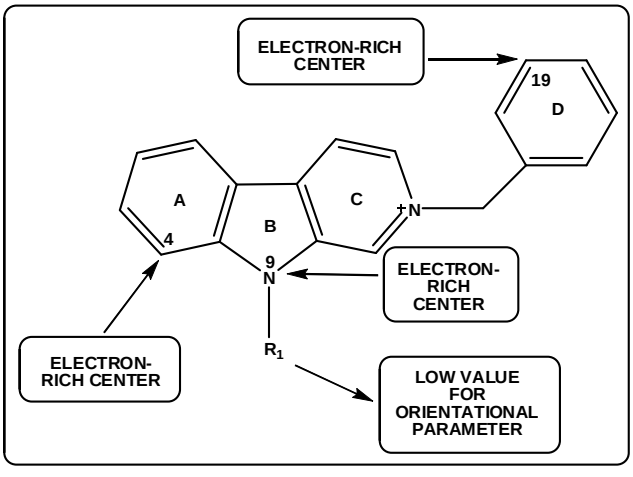

Figure 34. Partial 2D pharmacophore from Eq. 7.

HT-29 Cell Line
Group IA

Beta values (Table 12 and Fig. 4) indicate that the relative importance of the variables is $S_{17}^{E}(HOMO-2)*$ > $S_{10}^{E}(HOMO)*$ > $S_{18}^{N}(LUMO+1)*$ > S_{14}^{N}>. A VbV analysis shows that a low cytotoxicity is associated with high values for $S_{17}^{E}(HOMO-2)*$, $S_{18}^{N}(LUMO+1)*$ and S_{14}^{N}; and with a low value for $S_{10}^{E}(HOMO)*$. A high value for $S_{17}^{E}(HOMO-2)*$ ($(HOMO-2)_{17}^{*}$ is a σ or π MO, Table 24) is obtained by shifting upwards the MO energy. We suggest that this atom is interacting with an electron-deficient center with at least its two highest occupied MOs and that an optimal situation occurs when $(HOMO-2)_{17}^{*}$ is of π nature. A high value for $S_{18}^{N}(LUMO+1)*$ ($(LUMO+1)_{18}^{*}$ is a π MO, Table 25) is an indication that atom 18 is interacting with an electron-rich center through its two lowest vacant MOs. A low value for $S_{10}^{E}(HOMO)*$ suggests that this atom is interacting with an electron-rich center. S_{14}^{N} will not be discussed due to its high p value (Table 12). Fig. 35 shows the associated pharmacophore.

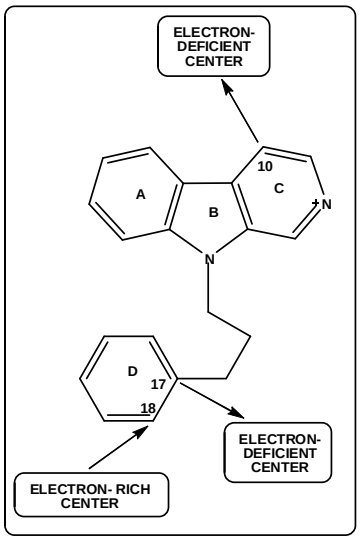

Figure 35. Partial 2D pharmacophore from Eq. 8.

Group IB

Beta values (Table 13) indicate that the relative importance of the variables is $S_{9}^{N}(LUMO)*$ > $\phi_{R1} = F_{19}(LUMO+2)*$ > $F_{15}(LUMO+2)*$. A VbV analysis shows that a low cytotoxicity is associated with high values for $F_{15}(LUMO+2)*$ and with low values for $S_{9}^{N}(LUMO)*$, $F_{19}(LUMO+2)*$ and ϕ_{R1}. $F_{15}(LUMO+2)*$ will not be discussed because of its high p value (Table 13). A low numerical value for $S_{9}^{N}(LUMO)*$ ($(LUMO)_{9}^{*}$ is of π nature, Table 27) suggests that atom 9 is interacting with an electron-rich center. A low value for $F_{19}(LUMO+2)*$ ($(LUMO+2)_{19}^{*}$ is a π MO, Table 28) can be interpreted by suggesting that atom 19 is interacting with an electron-rich center through its first two lowest vacant MOs and that $(LUMO+2)_{19}^{*}$ is engaged in a repulsive interaction with a σ MO of the partner. Without forgetting that ring D seems to interact with an extra site, a low value for ϕ_{R1} can be obtained, as we said before, with CH_3, C_2H_5 and similar substituents. Fig. 36 shows the associated pharmacophore.

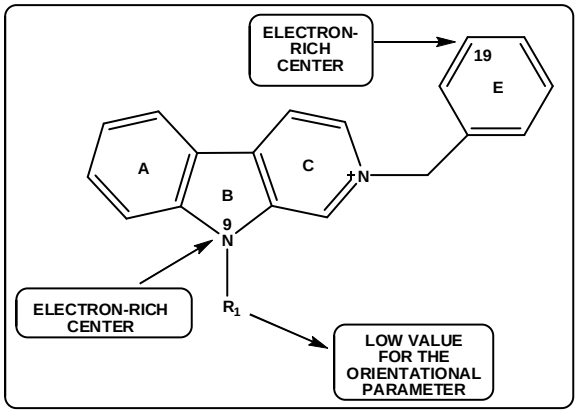

Figure 36. Partial 2D pharmacophore from Eq. 9.

769-P Cell Line
Group IB

Beta values (Table 14) indicate that the relative importance of the variables is $F_7(HOMO-2)*$ > $F_{16}(HOMO)*$ > $F_{17}(LUMO)*$ > $S_4^E(HOMO-2)*$. A VbV analysis shows that a low cytotoxicity is associated with high values for $F_7(HOMO-2)*$ and $S_4^E(HOMO-2)*$; and with low values for $F_{16}(HOMO)*$ and $F_{17}(LUMO)*$. A high value for $F_7(HOMO-2)*$ ($(HOMO-2)_7^*$ is a π MO, Table 26) indicates that atom 17 is interacting with an electron-deficient center through its three lowest vacant MOs. The first three highest occupied local MOs of atom 4 are of π nature (Table 26). A high value for $S_4^E(HOMO-2)*$ strongly suggests that atom 4 is interacting with an electron-deficient center through its three highest occupied MOs. A low value for $F_{16}(HOMO)*$ indicates that this atom is interacting with an electron-rich center. The case of atom 17, where a low value for $F_{17}(LUMO)*$ is required, suggests an interaction with an electron-deficient center. Fig. 37 shows the associated pharmacophore.

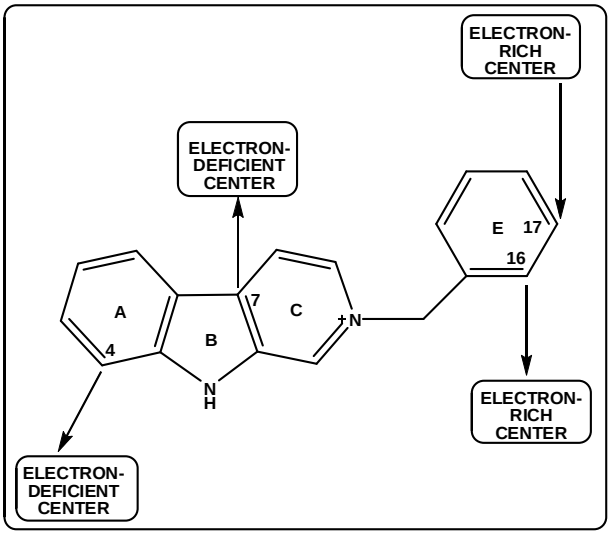

Figure 37. Partial 2D pharmacophore from Eq. 10.

A375 Cell Line

Group IA

Beta values (Table 15) indicate that the relative importance of the variables is $S_{17}^{E}(HOMO-2)* = S_{10}^{N} > F_{14}(LUMO+1)* > F_{16}(LUMO+2)* = \mu_6$. A VbV analysis shows that a low cytotoxicity is associated with high values for $S_{17}^{E}(HOMO-2)*$ and $F_{16}(LUMO+2)*$; and with low values for S_{10}^{N}, μ_6 and $F_{14}(LUMO+1)*$. A high value for $S_{17}^{E}(HOMO-2)*$ ($(HOMO-2)_{17}^{*}$ is a σ MO in most molecules, Table 24) suggest that a π MO will help $(HOMO-1)_{17}^{*}$ and $(HOMO)_{17}^{*}$, both of π character, to interact with an electron-deficient center. It is possible that a σ MO could engage in a repulsive interaction with other occupied σ MOs of the partner [110, 111]. Atom 16 is a carbon of a CH_2 group and has only σ MOs. A high value for $F_{16}(LUMO+2)*$ can be interpreted as an attractive interaction with occupied σ MOs. A low value for S_{10}^{N} suggests that atom 10 is interacting with an electron-deficient center. μ_6 is the midpoint between the energies el the local $(HOMO)_6^{*}$ and $(LUMO)_6^{*}$ MOs. A lower (i.e., a more negative) value for μ_6 can be obtained by lowering the $(LUMO)_6^{*}$ energy. This suggests that atom 6 is interacting with an electron-rich center. A low value for $F_{14}(LUMO+1)*$ ($(LUMO+1)_{14}^{*}$ is a σ MO, Table 24) is interpreted as a repulsive interaction between empty σ MOs [110, 111]. Fig. 38 shows the resultant pharmacophore.

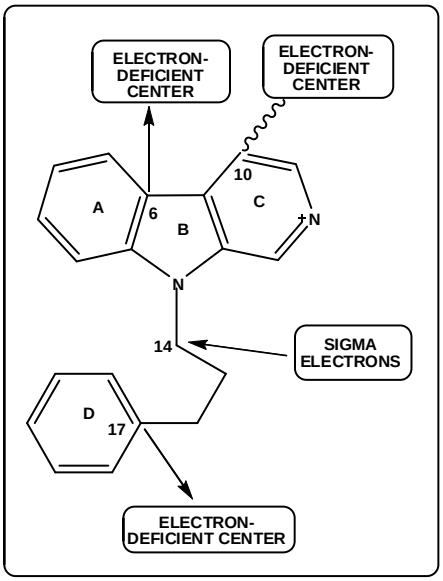

Figure 38. Partial 2D pharmacophore from Eq. 11.

Group IB

Beta values (Table 16) indicate that the relative importance of the variables is $\phi_{R1} > S_4^N > \eta_{18} > F_9(HOMO-1)* > S_{14}^{N}(LUMO+2)* > Q_{16}$. A VbV analysis shows that a low cytotoxicity is associated with positive values for Q_{16}, high values for $F_9(HOMO-1)*$ and low values for S_4^N, ϕ_{R1}, η_{18} and $S_{14}^{N}(LUMO+2)*$. A high value for $F_9(HOMO-1)*$ ($(HOMO-1)_9^{*}$ is a π MO, Table 27) suggests that atom 9 is interacting with an electron-deficient center through its first two highest occupied MOs. A low value for S_4^N indicates that atom 4 interacts with an electron-deficient center. A low value for η_{18} suggests that atom 18 interacts with an electron-rich center. A low value for $S_{14}^{N}(LUMO+2)*$ ($(LUMO+2)_{14}^{*}$ is a σ MO, Table 27)

suggests that atom 14 is engaged in an attractive interaction with occupied σ MOs of the partner. A low value for ϕ_{R1} suggests that CH_3, C_2H_5 and similar substituents will be suitable for low cytotoxicity. Fig. 39 shows the resultant pharmacophore.

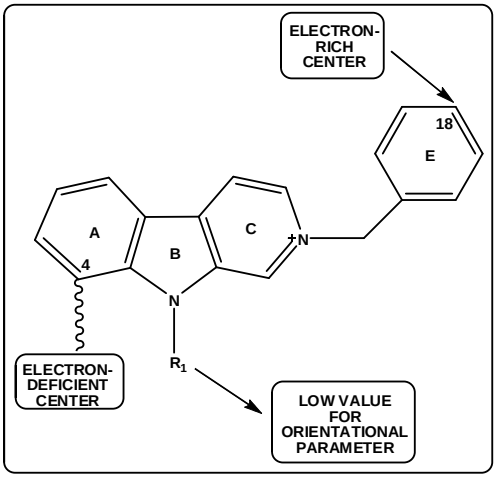

Figure 39. Partial 2D pharmacophore from Eq. 12.

SK-OV-3 Cell Line
Group IA

Beta values (Table 17) indicate that the relative importance of the variables is $\eta_{21} > \phi_{R2} > F_{22}(HOMO)*$. A VbV analysis shows that a low cytotoxicity is associated with high values for ϕ_{R2} and $F_{22}(HOMO)*$; and with low values for η_{21}. A low value for η_{21} suggests that this atom is interacting with an electron-rich center. ϕ_{R2} is a purely geometrical index and a high numerical value for it could influence the percentage of molecules having the appropriate rotational velocity interval allowing a proper interaction with the site. A low value for $F_{22}(HOMO)*$ ($(HOMO)^*_{22}$ is a π MO, Table 25) can be interpreted as the interaction of atom 22 with an electron-rich center. Fig. 40 shows the resultant pharmacophore.

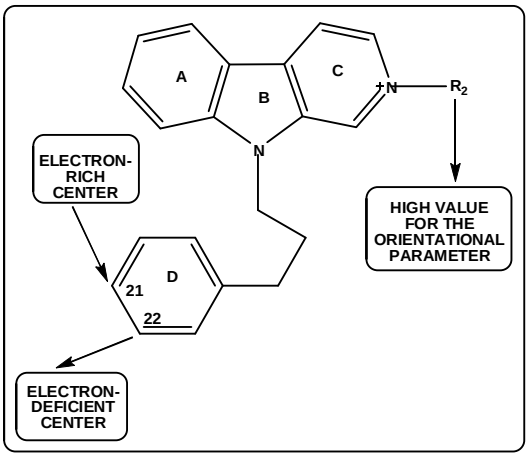

Figure 40. Partial 2D pharmacophore from Eq. 13.

Group IB

Beta values (Table 18) indicate that the relative importance of the variables is $\phi_{R1} > S_{18}^{E}(HOMO-1)* > S_{11}^{N} > Q_8 = F_3(HOMO-1)*$. A VbV analysis shows that a low cytotoxicity is associated with negative values for Q_8, high values for $S_{18}^{E}(HOMO-1)*$ and $F_3(HOMO-1)*$; and low values for S_{11}^{N} and ϕ_{R1}. A high value for $S_{18}^{E}(HOMO-1)*$ ($(HOMO-1)_{18}^{*}$ is a π MO, Table 28) suggests that atom 18 is interacting with an electron-deficient moiety. This is the same case for atom 3. A low value for S_{11}^{N} indicates that atom 11 interacts with an electron-rich center. A low value for ϕ_{R1}, as said before, suggests that CH_3, C_2H_5 and similar small substituents will be suitable for low cytotoxicity. Fig. 41 shows the resultant pharmacophore.

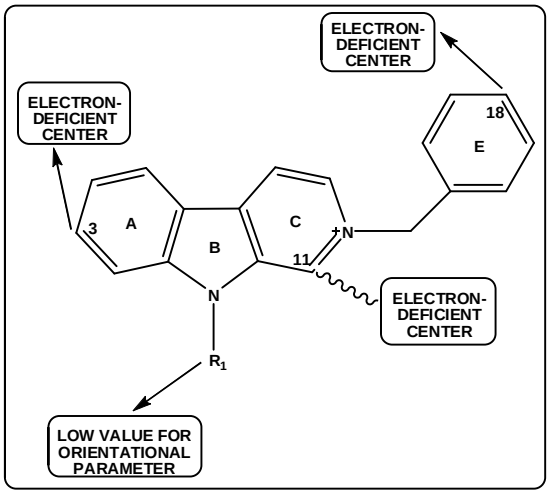

Figure 41. Partial 2D pharmacophore from Eq. 14.

Eca-109 Cell Line
Group IA

Beta values (Table 19) indicate that the relative importance of the variables is $F_8(LUMO+2)* > F_{16}(HOMO-1)* > S_{10}^{N}(LUMO)* > F_{11}(LUMO)*$. A VbV analysis shows that a low cytotoxicity is associated with high values for $F_8(LUMO+2)*$, $F_{16}(HOMO-1)*$ and $F_{11}(LUMO)*$; and with low values for $S_{10}^{N}(LUMO)*$. A high value for $F_8(LUMO+2)*$ ($(LUMO+2)_8^{*}$ is a π MO in almost all molecules, Table 22) strongly suggests that atom 8 interacts with an electron-rich center. This interaction seems to occur through at least the two lowest vacant MOs. A high value for $F_{16}(HOMO-1)*$ ($(HOMO-1)_{16}^{*}$ is a σ MO, Table 24) suggests an attractive interaction between the first two highest occupied MOs of atom 16 and one or more vacant σ MOs. A high value for $F_{11}(LUMO)*$ is associated with the interaction of atom 11 with an electron-rich center. A low value for $S_{10}^{N}(LUMO)*$ ($(LUMO)_{10}^{*}$ is a π MO, Table 24) points to an interaction with an electron-deficient center. Fig. 42 shows the resultant pharmacophore.

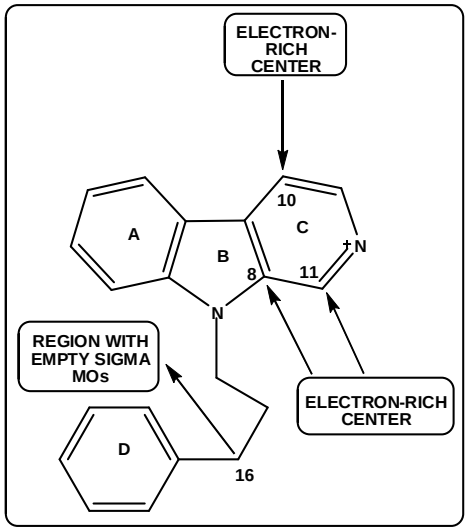

Figure 42. Partial 2D pharmacophore from Eq. 15.

BGC-823 Cell Line
Group IA

Beta values (Table 20) indicate that the relative importance of the variables is $Q_2 > S_{16}^E(HOMO-1)* > F_{16}(LUMO+1)* > \eta_8$. A VbV analysis shows that a low cytotoxicity is associated with positive values for Q_2, high values for $S_{16}^E(HOMO-1)*$ and $F_{16}(LUMO+1)*$; and with low values for η_8. A high value for $S_{16}^E(HOMO-1)*$ ($(HOMO-1)_{16}^*$ is a σ MO, Table 24) suggests an interaction of the first two highest occupied MOs of atom 16 with vacant σ MOs of a moiety. A high value for $F_{16}(LUMO+1)*$ ($(LUMO+1)_{16}^*$ is a σ MO, Table 24) suggests that atom 16 also interacts with a region with occupied σ MOs. We have not enough information to affirm that the site is the same for both interactions of atom 16 or that this atom is facing two or more CH_2 groups. A low value for η_8 is indicative of an interaction of atom 8 with an electron-rich center. A positive value for Q_2 suggests that atom 2 is close to a negatively-charged group. Fig. 43 shows the resultant pharmacophore.

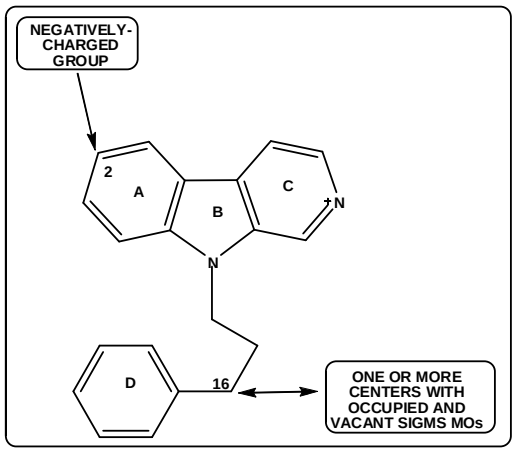

Figure 43. Partial 2D pharmacophore from Eq. 16.

Group IB

Beta values (Table 21) indicate that the relative importance of the variables is $s_{17} = Q_4 > \phi_{R1} > F_{16}(HOMO)* > s_{10}$. A VbV analysis shows that a low cytotoxicity is associated with high values for s_{17} and Q_4; and with low values for ϕ_{R1}, s_{10} and $F_{16}(HOMO)*$. A positive value for Q_4 indicates that atom 4 is facing a negatively-charged center. A high value for s_{17} indicates that this atom behaves as a good electron acceptor and that it is probably facing an electron-rich center. A low value for ϕ_{R1}, as said before, is interpreted asserting that CH_3 and similar small alkyl substituents are suitable for low cytotoxicity. A low value for s_{10} suggests that atom 10 is interacting with an electron-rich center. Fig. 44 shows the resultant pharmacophore.

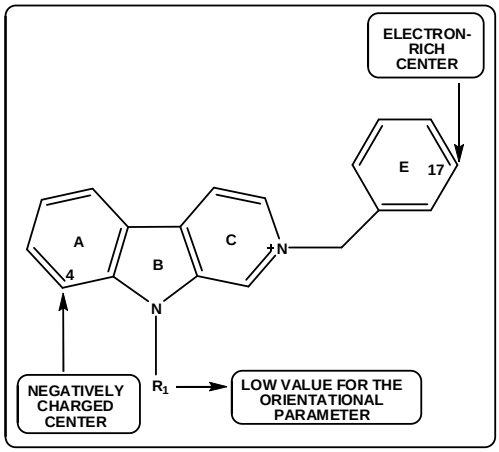

Figure 44. Partial 2D pharmacophore from Eq. 17.

We stated in a paper that "*if good QSAR results are not obtained, at least two possibilities should be considered. The first one is a reformulation of the composition of the common skeleton. The second one is related to the fact that some molecules could exert their biological action via different mechanisms*" [86]. We were not able to obtain statistically significant equations for the whole set. After dividing the set into two subsets, each one with its own common skeleton, satisfactory results were obtained. Nevertheless for two cases (for group IA against the 769-P cell line and for group IB against the Eca-109 cell line) it was impossible to obtain any result. A possible, but not necessarily true explanation is that in these cases we face different action mechanisms. The plots of experimental *versus* calculated values (Figs. 6-21) indicate that the hypothesis that the majority of the cytotoxic activity is encoded in the two common skeletons considered is reasonable. In several cases, it is highly probable that some molecules interact with the site through atoms that are not included in the common skeleton. At the light of the above results, is it possible to propose definite atoms as targets for substitution? We think that marking the number of times that a given atom appears in the resulting equations can provide a first answer. Figures 44 and 45 show, respectively, the results of the procedure.

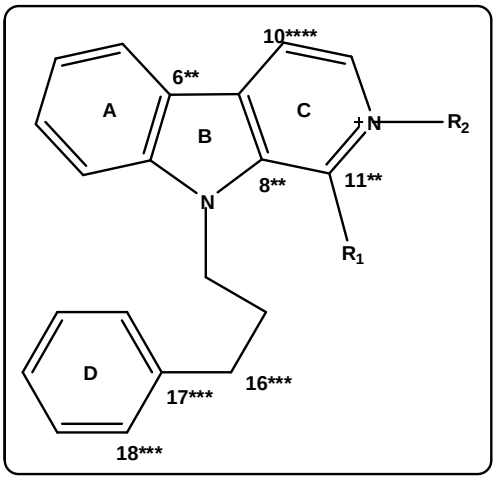

Figure 44. Atoms of group IA that are possible targets for substitution.

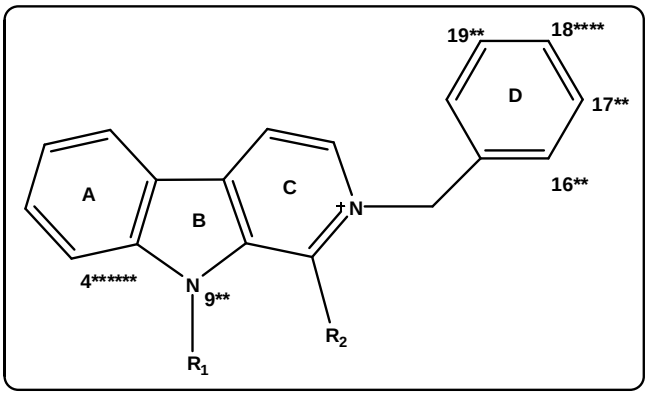

Figure 45. Atoms of group IA that are possible targets for substitution.

We can see that in the two groups the primary target atoms are not the same. We think that these atoms are possibly important targets to study.

Acknowledgements
This research work was carried out by Mr. Fernando Gatica-Díaz under the supervision of Dr. Juan S. Gómez-Jeria.

REFERENCES

[1] DN Stephens, *Anxiolytic [Beta]-carbolines : from molecular biology to the clinic*, Springer-Verlag, Berlin ; New York, **1993**.
[2] L Antkiewicz-Michaluk; H Rommelspacher, *Isoquinolines and beta-carbolines as neurotoxins and neuroprotectants : new vistas in Parkinson's disease therapy*, Springer, New York, **2012**.
[3] BC Labate, *Ayahuasca shamanism in the Amazon and beyond*, Oxford University Press, Oxford ; New York, **2014**.
[4] BC Labate; EJBdN Macrae, *Ayahuasca, ritual and religion in Brazil*, Equinox, London ; Oakville, Conn., **2010**.
[5] JP Harpignies, *Visionary plant consciousness : the Shamanic teachings of the plant world*, Park Street Press, Rochester, Vt., **2007**.
[6] R Metzner, *Sacred vine of spirits : ayahuasca*, Park Street Press, Rochester, Vt., **2006**.
[7] R Metzner; JC Callaway, *Ayahuasca : hallucinogens, consciousness, and the spirit of nature*, Thunder's Mouth Press, New York, **1999**.
[8] FC Savariz; MA Foglio; ALT Goes Ruiz; WF da Costa; M de Magalhães Silva, et al., *Bioorg. Med. Chem.*, **2014**, 22, 6867-6875.

[9] S Manda; SI Khan; SK Jain; S Mohammed; BL Tekwani, et al., *Bioorg. Med. Chem. Lett.*, **2014**, 24, 3247-3250.
[10] KA Mahmoud; M Krug; T Wersig; I Slynko; C Schächtele, et al., *Bioorg. Med. Chem. Lett.*, **2014**, 24, 1948-1951.
[11] X Han; J Zhang; L Guo; R Cao; Y Li, et al., *PLoS ONE*, **2012**, 7, e46546.
[12] K Huber; L Brault; O Fedorov; C Gasser; P Filippakopoulos, et al., *J. Med. Chem.*, **2011**, 55, 403-413.
[13] D Frost; B Meechoovet; T Wang; S Gately; M Giorgetti, et al., *PLoS ONE*, **2011**, 6, e19264.
[14] Z Chen; R Cao; B Shi; L Guo; J Sun, et al., *Eur. J. Med. Chem.*, **2011**, 46, 5127-5137.
[15] W Yin; S Majumder; T Clayton; S Petrou; ML VanLinn, et al., *Bioorg. Med. Chem.*, **2010**, 18, 7548-7564.
[16] BKS Yeung; B Zou; M Rottmann; SB Lakshminarayana; SH Ang, et al., *J. Med. Chem.*, **2010**, 53, 5155-5164.
[17] Y Rook; K-U Schmidtke; F Gaube; D Schepmann; B Wünsch, et al., *J. Med. Chem.*, **2010**, 53, 3611-3617.
[18] JF Miller; EM Turner; RG Sherrill; K Gudmundsson; A Spaltenstein, et al., *Bioorg. Med. Chem. Lett.*, **2010**, 20, 256-259.
[19] C Ma; R Cao; B Shi; X Zhou; Q Ma, et al., *Eur. J. Med. Chem.*, **2010**, 45, 5513-5519.
[20] F Liu; L-Q Yu; C Jiang; L Yang; W-T Wu; Q-D You, *Bioorg. Med. Chem.*, **2010**, 18, 4167-4177.
[21] R Kumar; S Khan; A Verma; S Srivastava; P Viswakarma, et al., *Eur. J. Med. Chem.*, **2010**, 45, 3274-3280.
[22] Z Chen; R Cao; B Shi; W Yi; L Yu, et al., *Bioorg. Med. Chem. Lett.*, **2010**, 20, 3876-3879.
[23] A Bridoux; R Millet; J Pommery; N Pommery; J-P Henichart, *Bioorg. Med. Chem.*, **2010**, 18, 3910-3924.
[24] PA Barsanti; W Wang; Z-J Ni; D Duhl; N Brammeier, et al., *Bioorg. Med. Chem. Lett.*, **2010**, 20, 157-160.
[25] J Zhang; Y Li; L Guo; R Cao; P Zhao, et al., *Cancer Biol. Ther.*, **2009**, 8, 2374-2383.
[26] C Wernicke; Y Schott; C Enzensperger; G Schulze; J Lehmann; H Rommelspacher, *Biochemical Pharmacology*, 2007, 74, 1065-1077.
[27] Y Li; F Liang; W Jiang; F Yu; R Cao, et al., *Cancer Biol. Ther.*, **2007**, 6, 1204-1210.
[28] X Dong; Y Xu; C Afonso; W Jiang; JY Laronze, et al., *Bioorg. Med. Chem. Lett.*, **2007**, 17, 2549-2553.
[29] A Kumar; SB Katiyar; S Gupta; PMS Chauhan, *Eur. J. Med. Chem.*, **2006**, 41, 106-113.
[30] N Sunder-Plassmann; V Sarli; M Gartner; M Utz; J Seiler, et al., *Bioorg. Med. Chem.*, **2005**, 13, 6094-6111.
[31] A Miralles; S Esteban; A Sastre-Coll; D Moranta; VJ Asensio; JA García-Sevilla, *Eur. J. Pharmacol.*, **2005**, 518, 234-242.
[32] M Laronze; M Boisbrun; S Léonce; B Pfeiffer; P Renard, et al., *Bioorg. Med. Chem.*, **2005**, 13, 2263-2283.
[33] M Zhao; C Wang; Y Wu; K Zhou; S Peng, *Prep. Biochem. Biotech.*, **2004**, 34, 57-76.
[34] RA Glennon; B Grella; RJ Tyacke; A Lau; J Westaway; AL Hudson, *Bioorg. Med. Chem. Lett.*, **2004**, 14, 999-1002.
[35] S Begum; SI Hassan; BS Siddiqui, *Nat. Prod. Res.*, **2004**, 18, 341-347.
[36] Z Sui; J Guan; MJ Macielag; W Jiang; Y Qiu, et al., *Bioorg. Med. Chem. Lett.*, **2003**, 13, 761-765.
[37] AC Castro; LC Dang; F Soucy; L Grenier; H Mazdiyasni, et al., *Bioorg. Med. Chem. Lett.*, **2003**, 13, 2419-2422.
[38] Y Song; J Wang; SF Teng; D Kesuma; Y Deng, et al., *Bioorg. Med. Chem. Lett.*, **2002**, 12, 1129-1132.
[39] E Arzel; P Rocca; P Grellier; M Labaeïd; F Frappier, et al., *J. Med. Chem.*, **2001**, 44, 949-960.
[40] RA Glennon; M Dukat; B Grella; S-S Hong; L Costantino, et al., *Drug Alc. Depend.*, **2000**, 60, 121-132.
[41] B Bai; X-Y Li; L Liu; Y Li; H-J Zhu, *Bioorg. Med. Chem. Lett.*, **2014**, 24, 96-98.
[42] R Cao; X Guan; B Shi; Z Chen; Z Ren, et al., *Eur. J. Med. Chem.*, **2010**, 45, 2503-2515.
[43] Z Chen; R Cao; B Shi; W Yi; L Yu, et al., *Chem. Pharm. Bull.*, **2010**, 58, 901-907.
[44] Z Chen; R Cao; L Yu; B Shi; J Sun, et al., *Eur. J. Med. Chem.*, **2010**, 45, 4740-4745.
[45] R Kumar; L Gupta; P Pal; S Khan; N Singh, et al., *Eur. J. Med. Chem.*, **2010**, 45, 2265-2276.
[46] LPP Liew; JM Fleming; A Longeon; E Mouray; I Florent, et al., *Tetrahed.*, **2014**, 70, 4910-4920.
[47] L Liu; YY Xu; ZQ Yang; JN Xiang; GY Xu, *Chin. Chem. Lett.*, **2012**, 23, 1230-1232.
[48] C Ma; R Cao; B Shi; S Li; Z Chen, et al., *Eur. J. Med. Chem.*, **2010**, 45, 1515-1523.
[49] A Peduto; V More; P de Caprariis; M Festa; A Capasso, et al., *Mini Rev. Med. Chem.*, **2011**, 11, 486-491.
[50] FC Savariz; MA Foglio; JE de Carvalho; ALTG Ruiz; MCT Duarte, et al., *Molec.*, **2012**, 17, 6100-6113.
[51] B Shi; R Cao; W Fan; L Guo; Q Ma, et al., *Eur. J. Med. Chem.*, **2013**, 60, 10-22.
[52] Q Wu; Z Bai; Q Ma; W Fan; L Guo, et al., *MedChemComm.*, **2014**, 5, 953-957.
[53] M-L Yang; P-C Kuo; T-L Hwang; W-F Chiou; K Qian, et al., *Bioorg. Med. Chem.*, **2011**, 19, 1674-1682.
[54] G Zhang; R Cao; L Guo; Q Ma; W Fan, et al., *Eur. J. Med. Chem.*, **2013**, 65, 21-31.
[55] JS Gómez Jeria, *Boll. Chim. Farmac.*, **1982**, 121, 619-625.
[56] JS Gómez-Jeria, *Int. J. Quant. Chem.*, **1983**, 23, 1969-1972.
[57] JS Gómez-Jeria, "Modeling the Drug-Receptor Interaction in Quantum Pharmacology," in *Molecules in Physics, Chemistry, and Biology*, J. Maruani Ed., vol. 4, pp. 215-231, Springer Netherlands, **1989**.

[58] JS Gómez-Jeria; M Ojeda-Vergara; C Donoso-Espinoza, *Mol. Engn.*, **1995**, 5, 391-401.
[59] JS Gómez-Jeria; M Ojeda-Vergara, *J. Chil. Chem. Soc.*, **2003**, 48, 119-124.
[60] JS Gómez-Jeria, *Elements of Molecular Electronic Pharmacology (in Spanish)*, Ediciones Sokar, Santiago de Chile, **2013**.
[61] JS Gómez-Jeria, *Canad. Chem. Trans.*, **2013**, 1, 25-55.
[62] JS Gómez-Jeria; M Flores-Catalán, *Canad. Chem. Trans.*, **2013**, 1, 215-237.
[63] JS Gómez-Jeria, *Der Pharm. Lett.*, **2014**, 6., 95-104.
[64] JS Gómez-Jeria, *SOP Trans. Phys. Chem.*, **2014**, 1, 10-28.
[65] JS Gómez-Jeria; L Espinoza, *Bol. Soc. Chil. Quím.*, **1982**, 27, 142-144.
[66] JS Gómez-Jeria; D Morales-Lagos, "The mode of binding of phenylalkylamines to the Serotonergic Receptor," in *QSAR in design of Bioactive Drugs*, M. Kuchar Ed., pp. 145-173, Prous, J.R., Barcelona, Spain, **1984**.
[67] JS Gómez-Jeria; DR Morales-Lagos, *J. Pharm. Sci.*, **1984**, 73, 1725-1728.
[68] JS Gómez-Jeria; D Morales-Lagos; JI Rodriguez-Gatica; JC Saavedra-Aguilar, *Int. J. Quant. Chem.*, **1985**, 28, 421-428.
[69] JS Gómez-Jeria; D Morales-Lagos; BK Cassels; JC Saavedra-Aguilar, *Quant. Struct.-Relat.*, **1986**, 5, 153-157.
[70] JS Gómez-Jeria; BK Cassels; JC Saavedra-Aguilar, *Eur. J. Med. Chem.*, **1987**, 22, 433-437.
[71] JS Gómez-Jeria; P Sotomayor, *J. Mol. Struct. (Theochem)*, **1988**, 166, 493-498.
[72] JS Gómez-Jeria; M Ojeda-Vergara, *Int. J. Quant. Chem.*, **1997**, 61, 997-1002.
[73] JS Gómez-Jeria; L Lagos-Arancibia, *Int. J. Quant. Chem.*, **1999**, 71, 505-511.
[74] JS Gómez-Jeria; L Lagos-Arancibia; E Sobarzo-Sánchez, *Bol. Soc. Chil. Quím.*, **2003**, 48, 61-66.
[75] JS Gómez-Jeria; F Soto-Morales; G Larenas-Gutierrez, *Ir. Int. J. Sci.*, **2003**, 4, 151-164.
[76] JS Gómez-Jeria; LA Gerli-Candia; SM Hurtado, *J. Chil. Chem. Soc.*, **2004**, 49, 307-312.
[77] F Soto-Morales; JS Gómez-Jeria, *J. Chil. Chem. Soc.*, **2007**, 52, 1214-1219.
[78] JS Gómez-Jeria; F Soto-Morales; J Rivas; A Sotomayor, *J. Chil. Chem. Soc.*, **2008**, 53, 1393-1399.
[79] JS Gómez-Jeria, *J. Chil. Chem. Soc.*, **2010**, 55, 381-384.
[80] F Salgado-Valdés; JS Gómez-Jeria, *J. Quant. Chem.*, 2014, **2014** Article ID 431432, 1-15.
[81] C Barahona-Urbina; S Nuñez-Gonzalez; JS Gómez-Jeria, *J. Chil. Chem. Soc.*, **2012**, 57, 1497-1503.
[82] A Paz de la Vega; DA Alarcón; JS Gómez-Jeria, *J. Chil. Chem. Soc.*, **2013**, 58, 1842-1851.
[83] I Reyes-Díaz; JS Gómez-Jeria, *J. Comput. Methods Drug Des.*, **2013**, 3, 11-21.
[84] JS Gómez-Jeria, *Int. Res. J. Pure App. Chem.*, **2014**, 4, 270-291.
[85] JS Gómez-Jeria, *Brit. Microbiol. Res. J.*, **2014**, 4, 968-987.
[86] JS Gómez-Jeria, *Der Pharma Chem.*, **2014**, 6, 64-77.
[87] JS Gómez-Jeria, *Res. J. Pharmac. Biol. Chem. Sci.*, **2014**, 5, 2124-2142.
[88] JS Gómez-Jeria, *J. Comput. Methods Drug Des.*, **2014**, 4, 32-44.
[89] JS Gómez-Jeria, *Res. J. Pharmac. Biol. Chem. Sci.*, **2014**, 5, 424-436.
[90] JS Gómez-Jeria, *J. Comput. Methods Drug Des.*, **2014**, 4, 38-47.
[91] JS Gómez-Jeria, *Res. J. Pharmac. Biol. Chem. Sci.*, **2014**, 5, 780-792.
[92] JS Gómez-Jeria, *Submitted for Publication*, **2014**,
[93] JS Gómez-Jeria; J Molina-Hidalgo, *J. Comput. Methods Drug Des.*, **2014**, 4, 1-9.
[94] JS Gómez-Jeria; J Valdebenito-Gamboa, *Der Pharma Chem.*, **2014**, 6, 383-406.
[95] D Muñoz-Gacitúa; JS Gómez-Jeria, *J. Comput. Methods Drug Des.*, **2014**, 4, 33-47.
[96] D Muñoz-Gacitúa; JS Gómez-Jeria, *J. Comput. Methods Drug Des.*, **2014**, 4, 48-63.
[97] DI Pino-Ramírez; JS Gómez-Jeria, *Amer. Chem. Sci. J.*, **2014**, 4, 554-575.
[98] R Solís-Gutiérrez; JS Gómez-Jeria, *Res. J. Pharmac. Biol. Chem. Sci.*, **2014**, 5, 1401-1416.
[99] JS Gómez-Jeria; A Robles-Navarro, *Res. J. Pharmac. Biol. Chem. Sci.*, **2015**, 6, In press.
[100] MJ Frisch; GW Trucks; HB Schlegel; GE Scuseria; MA Robb, et al., Gaussian98 Rev. A.11.3, Gaussian, Pittsburgh, PA, USA, **2002**.
[101] JS Gómez-Jeria, *J. Chil. Chem. Soc.*, **2009**, 54, 482-485.
[102] JS Gómez-Jeria, D-Cent-QSAR: A program to generate Local Atomic Reactivity Indices from Gaussian log files. 1.0, Santiago, Chile, **2014**.
[103] Statsoft, Statistica 8.0, 2300 East 14 th St. Tulsa, OK 74104, USA, **1984-2007**.
[104] YC Martin, *Quantitative drug design: a critical introduction*, M. Dekker, New York, **1978**.
[105] T Bruna-Larenas; JS Gómez-Jeria, *Int. J. Med. Chem.*, **2012**, **2012** Article ID 682495, 1-16.
[106] U Varetto, Molekel 5.4.0.8, Swiss National Supercomputing Centre: Lugano, Switzerland, **2008**.

[107]RD Dennington; TA Keith; JM Millam, GaussViev 5.0.8, GaussViev 5.0.8, 340 Quinnipiac St., Bldg. 40, Wallingford, CT 06492, USA, **2000**-**2008**.
[108]Hypercube, Hyperchem 7.01, 419 Phillip St., Waterloo, Ontario, Canada, **2002**.
[109]Chemaxon, MarvinView, www.chemaxon.com, USA, **2014**.
[110]E Joselevich, *Ang. Chem. Int. Ed.*, **2004**, 43, 2992-2994.
[111]E Joselevich, *ChemPhysChem*, **2004**, 5, 619-624.